

# On the Robustness of AlphaFold: A COVID-19 Case Study

Ismail R. Alkhouri<sup>1</sup>, Sumit Jha<sup>2</sup>, Andre Beckus<sup>3</sup>, George Atia<sup>1</sup>, Rickard Ewertz<sup>1</sup>,  
Arvind Ramanathan<sup>4</sup>, Susmit Jha<sup>5</sup>, Alvaro Velasquez<sup>6</sup>

<sup>1</sup> Electrical & Computer Engineering Department, University of Central Florida, Orlando, FL 32816

<sup>2</sup> Computer Science Department, University of Texas at San Antonio, TX 78249

<sup>3</sup> Information Directorate, Air Force Research Laboratory, Rome, NY 13441

<sup>4</sup> Data Science and Learning, Argonne National Laboratory, Lemont, IL, 60439

<sup>5</sup> Computer Science Laboratory, SRI International, Menlo Park, CA, 94709

<sup>6</sup> Information Innovation Office, Defense Advanced Research Projects Agency, Arlington, VA 22203

## Abstract

Protein folding neural networks (PFNNs) such as AlphaFold predict remarkably accurate structures of proteins compared to other approaches. However, the robustness of such networks has heretofore not been explored. This is particularly relevant given the broad social implications of such technologies and the fact that biologically small perturbations in the protein sequence do not generally lead to drastic changes in the protein structure. In this paper, we demonstrate that AlphaFold does not exhibit such robustness despite its high accuracy. This raises the challenge of detecting and quantifying the extent to which these predicted protein structures can be trusted. To measure the robustness of the predicted structures, we utilize (i) the root-mean-square deviation (RMSD) and (ii) the Global Distance Test (GDT) similarity measure between the predicted structure of the original sequence and the structure of its adversarially perturbed version. We prove that the problem of minimally perturbing protein sequences to fool protein folding neural networks is **NP-complete**. Based on the well-established BLOSUM62 sequence alignment scoring matrix, we generate adversarial protein sequences and show that the RMSD between the predicted protein structure and the structure of the original sequence are very large when the adversarial changes are bounded by (i) 20 units in the BLOSUM62 distance, and (ii) five residues (out of hundreds or thousands of residues) in the given protein sequence. In our experimental evaluation, we consider 111 COVID-19 proteins in the Universal Protein resource (UniProt), a central resource for protein data managed by the European Bioinformatics Institute, Swiss Institute of Bioinformatics, and the US Protein Information Resource. These result in an overall GDT similarity test score average of around 34%, demonstrating a substantial drop in the performance of AlphaFold.

## Introduction

Proteins form the building blocks of life as they enable a variety of vital functions essential to life and reproduction. Naturally occurring proteins are bio-polymers typically composed of 20 amino acids and this primary sequence of amino acids is well known for many proteins, thanks to high-throughput sequencing techniques. However, in order to understand the functions of different protein molecules and complexes, it is essential to comprehend their three-dimensional (3D) structures. Until recently, one of the grand challenges in structural biology has been the accurate determination of the 3D structure of the protein from its primary sequence. Such accurate

ID: O43765  $n = 313$

RMSD = 12.051Å

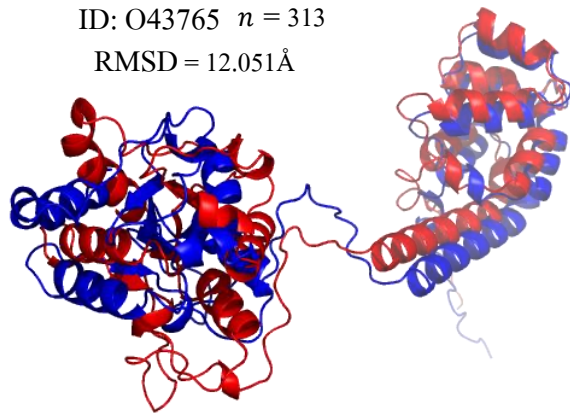


Figure 1: The structure of the original (black) and adversarial (red) sequences predicted using AlphaFold for the Small glutamine-rich tetratricopeptide repeat-containing protein alpha sequence. The length of the protein sequence is denoted by  $n$ . For structures, after their alignment using PyMol (Schrödinger and DeLano), the Root Mean Square Deviation (RMSD) is given in Angstroms (equal to  $10^{-10}$  meters and denoted by Å).

predictive protein folding promises to have a profound impact on the design of therapeutics for diseases and drug discovery (Chan et al. 2019).

AlphaFold (Jumper et al. 2021a) achieved unparalleled success in predicting protein structures using neural networks and remains first at the Critical Assessment of protein Structure Prediction (CASP14), which corresponds to year 2020, competition. While this has been touted as a breakthrough for structural biology (Bagdonas et al. 2021), the robustness of its predictions has not yet been explored. The main contribution of this paper is to demonstrate the susceptibility of AlphaFold to adversarial sequences by generating several examples where protein sequences that vary only in five residues out of hundreds or thousands of residues result in very different 3D protein structures. We present the problem of adversarial attacks on Protein Folding Neural Network (PFNN) and prove that the problem is **NP-complete**. We use sequence alignment scores (Henikoff and Henikoff 1992) such as those derived from Block Substitution Matrices (BLOSUM62) to identify a space of similar protein sequences used in constructing adversarial perturbations. For the output

structures, we leverage the standard metrics commonly used in CASP, namely (i) the root-mean-square deviation (RMSD) and (ii) the Global Distance Test (GDT) similarity measure between the predicted structure and the structure of its adversarially perturbed sequence. See Figure 1 and its caption for an example.

Moreover, we conduct two experiments investigating the choice of the BLOSUM threshold and the use of the prediction, per-residue, confidence information obtained from AlphaFold. Our experiments show that different input protein sequences have very different adversarial robustness as determined by the RMSD (GDT-TS) in the protein structure predicted by AlphaFold. These values range from 1.011Å (0.43%) to 49.531Å (98.8%) when the BLOSUM62 distance between the original and adversarial sequences is bounded by a threshold of 20 units with a hamming distance of 5 residues only. Hence, our proposed approach is a first step in the direction of identifying protein sequences on which the predicted 3D structure cannot be trusted.

## Summary and Related work

PFNNs (Jumper et al. 2021b; Baek et al. 2021) should be expected to obey the natural observation that biologically small changes in the sequence of a protein usually do not lead to drastic changes in the protein structure. Almost four decades ago, it was noted that two structures with 50% sequence identity align within approximately 1Å RMSD from each other (Chothia and Lesk 1986). Two proteins with even 40% sequence identity and at least 35 aligned residues align within approximately 2.5Å (Sander and Schneider 1991). The phenomenon of sequence-similar proteins producing similar structures have also been observed in larger studies (Rost 1999). As with almost any rule in biology, a small number of counterexamples to the conventional wisdom of similar sequences leading to similar structures do exist, wherein even small perturbations can potentially alter the entire fold of a protein. However, such exceptions are not frequent and often lead to exciting investigations (Cordes et al. 2000; Tuinstra et al. 2008).

Manipulating the multiple sequence alignment step of AlphaFold has been studied in (Stein and Mchaourab 2021) using in silico mutagenesis. However, there, the goal is not to study the robustness of the protein folding neural networks, but rather to enhance the prediction capability of AlphaFold in terms of the intrinsic conformational heterogeneity of proteins. The authors in (Del Alamo et al. 2022), present a method that manipulates inputs to obtain diverse distinct structures that are absent from the AlphaFold training data. Using membrane proteins, the authors show that their method enhances the multiple sequence alignment step while generating more accurate structures.

The work in (Jha et al. 2021) is aimed at generating adversarial sequences in order to cause significant damage to the output predicted structure of RosettaFold (Baek et al. 2021), which, according to CASP, is the second best protein folding neural network. However, the authors only show results for a few proteins and do not consider all the standard metrics for measuring the output structures. In contrast, in this paper, we

present results for more than 100 sequences, derive a complexity proof for the problem of finding adversarial protein sequences, and, based on the CASP competition, utilize all the standard metrics for measuring the output structures.

## Robustness Metric using Adversarial Attacks

The similar-sequence implies similar-structure paradigm dictates that PFNNs should make robust predictions. Given a protein sequence of  $n$  residues  $S = s_1 s_2 \dots s_n$  with a three-dimensional structure  $\mathcal{A}(S) = (x_1, y_1, z_1), \dots, (x_n, y_n, z_n)$ , we define a notion of biologically similar sequences  $\mathcal{V}$  using Block Substitution Matrices (BLOSUM) (Henikoff and Henikoff 1992), and then employ formulations of adversarial attacks (Goodfellow, McDaniel, and Papernot 2018) on PFNNs within this space of similar sequences to identify a sequence  $S_{\text{adv}} \in \mathcal{V}$  that produces a maximally different three-dimensional structure  $\mathcal{A}(S_{\text{adv}})$ . We then compute the RMSD and GDT between the structures for the original and adversarial inputs ( $\mathcal{A}(S)$  and  $\mathcal{A}(S_{\text{adv}})$ ), and use these metrics as the robustness measure. If the RMSD (GDT) is small (high), the response of the PFNN is deemed robust; a large (small) RMSD (GDT) indicates that the predicted structure is not robust.

## BLOSUM Similarity Measures

Given two sequences of  $n$  residues  $S = s_1 s_2 \dots s_n$  and  $S' = s'_1 s'_2 \dots s'_n$ , in which every residue  $s_i$  (or  $s'_i$ ) is from the set  $\mathcal{X} = \{A, R, N, D, C, Q, E, G, H, I, L, K, M, F, P, S, T, W, Y, V\}$  of amino acids, a natural question is how to compute the sequence similarity  $D_{\text{seq}}$  between these proteins. A naive approach would be to count the number of residues that are different, i.e., the Hamming distance. However, an analysis of naturally occurring proteins shows that not all changes in residues have the same impact on protein structures. Changes to one type of residue are more likely to cause structural variations than changes to another type of residue.

Early work in bioinformatics focused on properties of amino acids and reliance on genetic codes. However, more modern methods have relied on the creation of amino acid scoring matrices that are derived from empirical observations of frequencies of amino acid replacements in homologous sequences (Dayhoff, Schwartz, and Orcutt 1978; Jones, Taylor, and Thornton 1992). The original scoring matrix, called the PAM250 matrix, was based on empirical analysis of 1572 mutations observed in 71 families of closely-related proteins that are 85% or more identical after they have been aligned. The PAM1 model-based scoring matrix was obtained by normalizing the frequency of mutations to achieve a 99% identity between homologous proteins. These results were then extrapolated to create the PAM10, PAM30, PAM70 and PAM120 matrices with 90%, 75%, 55%, and 37% identity between homologous proteins.

Another interesting approach (Henikoff and Henikoff 1992) to understanding protein similarity is the direct counting of replacement frequencies using the so-called Block Substitution Matrices (BLOSUM). Instead of relying solely on sequences of homologous proteins that are relatively harder to find, the BLOSUM approach focuses on identifying conserved blocks or conserved sub-sequences in a larger variety

of proteins potentially unrelated by evolutionary pathways and counts the frequency of replacements within these conserved sub-sequences. BLOSUM62 (Figure 2), BLOSUM80 and BLOSUM90 denote block substitution matrices that are obtained from blocks or subsequences with at least 62%, 80%, and 90% similarity, respectively. The BLOSUM matrix  $[B_{ij}]$  is a matrix of integers where each entry denotes the similarity between residue of type  $b_i \in \mathcal{X}$  and type  $b_j \in \mathcal{X}$ .

We identify the space of biologically similar sequences  $\mathcal{V}$  for a given protein sequence  $S$  with respect to the BLOSUM distance. We expect the predicted structures for the similar sequences to be similar. If there is a large RMSD (or small GDT) between the predicted structure  $\mathcal{A}(S)$  and the structure of the adversarial sequence  $\mathcal{A}(S_{\text{adv}})$ , it would reflect a lack of robustness in the prediction of the network. We adopt a sequence similarity measure that counts replacement frequencies in conserved blocks across different proteins.

### Approach

Our approach to evaluating the robustness of PFNNs is based on two main ideas: (i) the existence of adversarial examples in PFNNs that produce adversarial structures possibly very different from the original structure, and (ii) the use of BLOSUM matrices for identifying a neighborhood of a given sequence that are biologically similar and hence expected to have similar 3D structures. We utilize the RMSD and GDT between the structure of an original protein sequence and the structure of the adversarial sequence as a measure of robustness of a protein folding network on the given input. In this work, we focus on the state-of-the-art AlphaFold model, the winner of the 1st place in CASP2020.

### Sequence Similarity Measures

Given two sequences  $S = s_1 s_2 \dots s_n$  and  $S' = s'_1 s'_2 \dots s'_n$ , the BLOSUM distance between the two sequences is given by Equation (1) below. For an illustrative example of  $D_{\text{seq}}$ , see Figure 3.

$$D_{\text{seq}}(S, S') = \sum_{i \in [n]} (B_{s_i s_i} - B_{s_i s'_i}) . \quad (1)$$

	A	R	N	D	C	Q	E	G	H	I	L	K	M	F	P	S	T	W	Y	V
A	4	-1	-2	0	-1	-1	0	-2	-1	-1	-1	-1	-2	-1	1	0	-3	-2	0	
R	-1	5	0	-2	-3	1	0	-2	0	-3	-2	2	-1	-3	-2	-1	-1	-3	-2	-3
N	-2	0	6	1	-3	0	0	1	-3	-3	0	-2	-3	-2	1	0	-4	-2	-3	
D	-2	-2	1	6	-3	0	2	-1	-1	-3	-4	-1	-3	-3	-1	0	-1	-4	-3	-3
C	0	-3	-3	-3	9	-3	-4	-3	-3	-1	-1	-3	-1	-2	-3	-1	-1	-2	-2	-1
Q	-1	1	0	0	-3	5	2	-2	0	-3	-2	1	0	-3	-1	0	-1	-2	-1	-2
E	-1	0	0	2	-4	2	5	-2	0	-3	-3	1	-2	-3	-1	0	-1	-3	-2	-2
G	0	-2	0	-1	-3	-2	-2	6	-2	-4	-4	-2	-3	-3	-2	0	-2	-2	-3	-3
H	-2	0	1	-1	-3	0	0	-2	8	-3	-3	-1	-2	-1	-2	-1	-2	-2	-2	-3
I	-1	-3	-3	-3	-1	-3	-3	-4	-3	4	2	-3	1	0	-3	-2	-1	-3	-1	3
L	-1	-2	-3	-4	-1	-2	-3	-4	-3	2	4	-2	2	0	-3	-2	-1	-2	-1	1
K	-1	2	0	-1	-3	1	1	-2	-1	-3	-2	5	-1	-3	-1	0	-1	-3	-2	-2
M	-1	-1	-2	-3	-1	0	-2	-3	-2	1	2	-1	5	0	-2	-1	-1	-1	-1	1
F	-2	-3	-3	-3	-2	-3	-3	-3	-1	0	0	-3	0	6	-4	-2	-2	1	3	-1
P	-1	-2	-2	-1	-3	-1	-1	-2	-2	-3	-3	-1	-2	-4	7	-1	-1	-4	-3	-2
S	1	-1	1	0	-1	0	0	0	-1	-2	-2	0	-1	-2	-1	4	1	-3	-2	-2
T	0	-1	0	-1	-1	-1	-1	-2	-2	-1	-1	-1	-1	-1	-2	-1	1	5	-2	-2
W	-3	-3	-4	-4	-2	-2	-3	-2	-2	-3	-2	-3	-1	1	-4	-3	-2	11	2	-3
Y	-2	-2	-2	-3	-2	-1	-2	-3	2	-1	-1	-2	-1	3	-3	-2	-2	2	7	-1
V	0	-3	-3	-3	-1	-2	-2	-3	-3	3	1	-2	1	-1	-2	-2	0	-3	-1	4

Figure 2: The BLOSUM62 matrix.

### Output Structural Measure

Given a sequence of  $n$  residues  $S = s_1 s_2 \dots s_n$ , its three dimensional structure  $\mathcal{A}(S)$  is an ordered  $n$ -tuple of three-dimensional co-ordinates  $(x_1, y_1, z_1), \dots, (x_n, y_n, z_n)$ . Our goal is to utilize a structural distance measure that captures the variations in the two structures  $\mathcal{A}(S)$  and  $\mathcal{A}(S')$  and is invariant to rigid-body motion. Therefore, in this work, we use standard structural distances, namely the RMSD, measured in Å, and the GDT with its two variants: (i) the Total Score (TS) and (ii) the High Accuracy (HA) (Zemla 2003).

Given the output structure of the adversarial sequence  $\mathcal{A}(S')$ , an alignment algorithm is employed before computing the RMSD and GDT measures between the two structures of interest. We use the alignment procedure implemented in PyMOL (Schrödinger and DeLano) to align  $\mathcal{A}(S')$  with regard to the target structure  $\mathcal{A}(S)$ . Let the aligned structure be denoted by  $\hat{\mathcal{A}}(S') = (\hat{x}'_1, \hat{y}'_1, \hat{z}'_1), \dots, (\hat{x}'_n, \hat{y}'_n, \hat{z}'_n)$ . Then, the RMSD, measured in Å, is obtained as

$$\text{RMSD}(\mathcal{A}(S), \hat{\mathcal{A}}(S')) = \sqrt{\frac{1}{n} \sum_{i \in [n]} d(\mathcal{A}(S)_i, \hat{\mathcal{A}}(S')_i)} , \quad (2)$$

where  $d(\mathcal{A}(S)_i, \hat{\mathcal{A}}(S')_i) = (x_i - \hat{x}'_i)^2 + (y_i - \hat{y}'_i)^2 + (z_i - \hat{z}'_i)^2$  and  $\mathcal{A}(S)_i$  represents the 3D carbon-alpha coordinates of the  $i^{\text{th}}$  residue. Using the carbon-alpha coordinates is the standard approach in CASP (Zemla 2003).

Another standard metric for gauging the similarity of protein structures is the GDT similarity measure, introduced by (Zemla 2003) and commonly used in the CASP competition along with the RMSD. In some cases, the latter is known to be sensitive to outliers (Zemla 2003). The GDT score returns a value in  $[0, 1]$  where 1 indicates identical structures, and is computed with respect to four thresholds,  $\delta_j$ , as

$$\text{GDT}(\mathcal{A}(S), \hat{\mathcal{A}}(S')) = \frac{1}{4n} \sum_{j \in [4]} \sum_{i \in [n]} \mathbf{1}(d(\mathcal{A}(S)_i, \hat{\mathcal{A}}(S')_i) < \delta_j) , \quad (3)$$

where the thresholds  $\delta_1, \delta_2, \delta_3$ , and  $\delta_4$  for TS (HA) are given by 1(0.5), 2(1), 4(2), and 8(4) for  $j$  equals to 1, 2, 3, and 4 respectively, and  $\mathbf{1}(\cdot)$  is the indicator function. In (3), each  $j \in [4]$  reflects the number of residues in the structures for which the distance is less than  $\delta_j$ .

### Adversarial Attacks on PFNNs

Small carefully crafted changes in a few pixels of input images cause well-trained neural networks with otherwise high accuracy to consistently produce incorrect responses in domains such as computer vision (Croce et al. 2020; Andriushchenko et al. 2020; Bai et al. 2020; Croce and Hein 2021). Given a neural network  $\mathcal{A}$  mapping a sequence  $S$  of residues to a three-dimensional geometry  $\mathcal{A}(S)$  describing the structure of the protein, we seek to obtain a sequence  $S'$  such that the sequence similarity measure  $D_{\text{seq}}(S, S')$  between  $S$  and  $S'$  is small and some structural distance measure  $D_{\text{str}}(\mathcal{A}(S), \mathcal{A}(S'))$  is maximized. This can be achieved by

Original and Adversarial Sequences

$S$		$D_{\text{seq}}$	$D_{\text{ham}}$
$S$	MDLFMRFFTLGSITAPVKIDNASPASTVHATATIPLQASLPFGWLIVIGVAFLAVFQSATKIIALNKRWQLALYKGFQFCINLLLLFVTIYSHLLLVAAG		
$S'_1$	DVPSMRFFTLGSITAPVKIDNASPASTVHATATIPLQASLPFGWLIVIGVAFLAVFQSATKIIALNKRWQLALYKGFQFCINLLLLFVTIYSHLLLVAAG	32	4
$S'_2$	FGCYMRFFTLGSITAPVKIDNASPASTVHATATIPLQASLPFGWLIVIGVAFLAVFQSATKIIALNKRWQLALYKGFQFCINLLLLFVTIYSHLLLVAAG	20	4
$S'_3$	MDLFMRFFTLGSITAPVIRVNPASASTVHATATIPLQASLPFGWLIVIGVAFLAVFQSATKIIALNKRWQLALYKGFQFCINLLLLFVTIYSHLLLVAAG	12	4
$S'_4$	MDLFMRFFTLGSITAPVKIDNASPASTVHATATIPLQASLWAYKLVIGVAFLAVFQSATKIIALNKRWQLALYKGFQFCINLLLLFVTIYSHLLLVAAG	42	4
$S'_5$	MDLFMRFFVIAAVTAQPVKIDNASPASTVHATATIPLQASLPFGWLIVIGVAFLAVFQSATKIIALNKRWQLALYKGFQFCINLLLLFVTIYSHLLLVAAG	17	5
$S'_6$	MDLFMRFFTLGSITAPVKIDNASPASTVHATATIPLQASDIERRLVIGVAFLAVFQSATKIIALNKRWQLALYKGFQFCINLLLLFVTIYSHLLLVAAG	49	5
$S'_7$	MDLFMRFFTLGSITAPVKIDNASPASTVHATATIPLQASLPFGWLIVIGVAFLAVFQSATRVLTMKKRWQLALYKGFQFCINLLLLFVTIYSHLLLVAAG	18	6
$S'_8$	MDLFMRFFTLGSITAPVKIDNASPASTVHATATIPLQAVEFQLVIVIGVAFLAVFQSATKIIALNKRWQLALYKGFQFCINLLLLFVTIYSHLLLVAAG	57	6
$S'_9$	MDLFMRFFTLGSITAPVKIDNASPASTVHATATIPLQASLPFGWLIVIGVAFLAVFQSATKIIALNKRWQLALYKGFQFCINLACMYISMVSHLLLVAAG	23	7
$S'_{10}$	MDLFMRFFTLGSITAPVKIDNASPASTVHATATIPLQASDIGIINGIVGVAFLAVFQSATKIIALNKRWQLALYKGFQFCINLLLLFVTIYSHLLLVAAG	65	7

Figure 3: The original sequence  $S$  is followed by 10 sequences generated by changing 4, 5, 6, and 7 residues. The sequences are samples from the space in (5) with different values of  $L$  and  $H$ . The distance  $D_{\text{seq}}$  is calculated using (1).

solving the following optimization problem

$$\max_{S'} D_{\text{str}}(\mathcal{A}(S), \mathcal{A}(S')) \text{ s.t. } D_{\text{seq}}(S, S') \leq L. \quad (4)$$

In our experiments, we set  $L = 20$  and  $D_{\text{str}}$  as the RMSD measure. Given the discrete nature of the input sequences, well-known methods for generating adversarial examples (e.g. gradient-based methods) fail to produce valid and accurate results. As such, we propose a solution based on a brute-force exploration in the space of biologically similar sequences that, given a sequence of interest  $S$  with  $n$  residues, can be defined as

$$\mathcal{V}_{L,H}(S) = \{S' \in \mathcal{X}^n \mid D_{\text{seq}}(S, S') \leq L \text{ and } D_{\text{ham}}(S, S') \leq H\}, \quad (5)$$

where  $\mathcal{X}^n$  is the set of all possible sequences over  $\mathcal{X}$  of length  $n$ ,  $D_{\text{ham}}$  is the hamming distance, and  $H$  is a predefined threshold. For long sequences, the search space can be extensively large. Therefore, we select random samples from  $\mathcal{V}_{L,H}(S)$  and choose the sequence that returns the maximum value based on the RMSD measure. Our approach to generating adversarial sequences falls under the class of black-box attacks. This means that we only have access to the output of the network (Papernot et al. 2017).

It is worth noting that the inference time of complex protein folding systems, which apply multiple processing and alignment steps prior to the use of any neural network, such as AlphaFold is extremely high compared to NN-based image classifiers. The forward pass of such systems involves a large number of computations. This fact, along with the discrete nature of the input space, are the bottleneck of developing more complex black-box attacks (Mahmood et al. 2021), which in general require a high number of queries.

## Complexity

In this section, we formalize the problem of generating an adversarial attack for PFNNs and establish its complexity.

**Definition 1** (PFNN Adversarial Attack (PAA) Problem). *Given a learning model  $\mathcal{A}(\cdot; \theta) : \mathcal{X}^n \rightarrow (\mathbb{R} \times \mathbb{R} \times \mathbb{R})^n$  mapping residues to 3-dimensional coordinates and parameterized by  $\theta$ , a sequence  $S \in \mathcal{X}^n$ , and a sequence alignment scoring matrix  $B$ , find an input sequence  $S' \in \mathcal{X}^n$  such that  $D_{\text{seq}}(S, S') \leq L$  and  $D_{\text{str}}(\mathcal{A}(S), \mathcal{A}(S')) \geq U$ , where the bounds  $L$  and  $U$  and distance functions  $d$  and  $D$  are given.*

We prove that the PAA problem is **NP-complete**. This establishes that, in general, there is no polynomial-time solution to the PAA problem unless  $\mathbf{P} = \mathbf{NP}$ . Due to this complexity and for ease of presentation, we adopt simple perturbation attacks for our experiments in the next section. We begin by defining the **NP-complete** problem to be reduced to an instance of the PAA problem.

**Definition 2** (CLIQUE Problem). *Given an undirected graph  $G = (V, E)$  and an integer  $k$ , find a fully connected subgraph induced by  $V' \subseteq V$  such that  $|V'| = k$ .*

**Theorem 1.** *The PFNN Adversarial Attack (PAA) problem in Definition 1 is NP-complete.*

*Proof.* It is easy to verify that the PAA problem is in **NP** since, given a solution sequence  $S'$ , one can check whether the constraints  $D_{\text{seq}}(S, S') \leq L$  and  $D_{\text{str}}(\mathcal{A}(S), \mathcal{A}(S')) \geq U$  are satisfied in polynomial time. It remains to be shown whether the PAA problem is **NP-hard**. We establish this result via a reduction from the CLIQUE problem in Definition 2. Given a CLIQUE instance  $\langle G = (V, E), k \rangle$  with  $|V| = n$  and  $|E| = m$ , we construct its corresponding PAA instance  $\langle \mathcal{A}(\cdot; \theta), S, B, L, U \rangle$  as follows. Without loss of generality, let us consider a restricted version of the PAA problem where there are only two residue types  $\{N, K\}$  with the corresponding BLOSUM62 sub-matrix  $B' = 6 \cdot I$ , where  $I$  denotes the identity matrix. Following the one-hot representation of residues adopted in (Jumper et al. 2021b), any input tensor over  $\{N, K\}$  is represented as a one-hot encoding  $S^{\text{in}} \in (\mathbb{B} \times \mathbb{B})^n$  to be used as an input tensor to  $\mathcal{A}$ , where  $s_{i0}^{\text{in}} = 1$  ( $s_{i1}^{\text{in}} = 1$ ) denotes that residue  $s_i^{\text{in}}$  is of type  $N$  ( $K$ ). Let  $S = (N, N, \dots, N)$  denote the all- $N$  sequence. We set  $L = 6k$  and  $U = \frac{k(k-1)}{2} \sqrt{\frac{3}{n}}$ . The connectivity structure of  $\mathcal{A}$  is derived from the edges  $E$  in the CLIQUE instance as follows. The first column of the input tensor corresponding to  $s_{i0}^{\text{in}}$  for all  $i \leq n$  is disconnected from the network and the second column corresponding to  $s_{i1}^{\text{in}}$  is connected to  $\mathcal{A}$  such that, for each edge  $(v_i, v_j) \in E$ , we have a connection from  $s_{i1}^{\text{in}}$  and  $s_{j1}^{\text{in}}$  to each of the three outputs in the first three-dimensional coordinate of  $\mathcal{A}(S^{\text{in}})_1$ . All connections have a weight of unity and this defines the parameters  $\theta$  of the model  $\mathcal{A}$ . Therefore, without loss of generality, we are only considering the first of the  $n$  output three-dimensional coordinates

$\mathcal{A}(S^{\text{in}})_1$ . In particular, these values keep track of the number of edges induced by the vertices in  $G$  corresponding to the non-zero entries in  $s_{11}^{\text{in}}, \dots, s_{1n}^{\text{in}}$ . We now prove that there is a clique of size  $k$  in  $G$  if and only if there is a feasible solution  $S^{\text{in}} = S'$  to the reduced PAA instance.

( $\implies$ ) Assume there is a clique of size  $k$  in  $G$ . We can derive a feasible solution  $S'$  to the reduced PAA instance as follows. For every vertex  $v_i \in V$  (not) in the clique, let  $(s'_{i0} = 1) s'_{i1} = 1$ . Since  $S$  is the all- $N$  sequence, its corresponding one-hot encoding consists of  $s_{i0} = 1$  for all  $1 \leq i \leq n$ . Thus, the corresponding BLOSUM62 distance is

$$D_{\text{seq}}(S, S') = \sum_{1 \leq i \leq n} (6 - 6 \cdot \mathbf{1}(s_i \neq s'_i)) = 6k. \quad (6)$$

This satisfies the sequence alignment constraint defined by  $D_{\text{seq}}(S, S') \leq L = 6k$ . Furthermore, the solution  $S'$  induces outputs of  $x'_1 = y'_1 = z'_1 = k(k-1)/2$ , leading to an RMSD of  $U$ . Without loss of generality, we omit the alignment step in computing the RMSD and therefore assume that  $\mathcal{A}(S') = \hat{\mathcal{A}}(S')$ . The corresponding RMSD distance  $D_{\text{str}}(\mathcal{A}(S), \hat{\mathcal{A}}(S'))$  in output predictions is presented below. Recall that  $x_1 = y_1 = z_1 = 0$  for the the all- $N$  sequence  $S$  because its corresponding column in the one-hot encoding is disconnected from the network.

$$\begin{aligned} D_{\text{str}}(\mathcal{A}(S), \mathcal{A}(S')) &= \sqrt{\frac{1}{n} \sum_{i \in [n]} d(\mathcal{A}(S)_i, \hat{\mathcal{A}}(S')_i)} \\ &= \sqrt{\frac{1}{n} \left[ 3 \left( 0 - \frac{k(k-1)}{2} \right)^2 \right]} = \frac{k(k-1)}{2} \sqrt{\frac{3}{n}}. \end{aligned} \quad (7)$$

Thus, the constraint  $D_{\text{str}}(S, S') \geq U = \frac{k(k-1)}{2} \sqrt{\frac{3}{n}}$  is satisfied.

( $\impliedby$ ) We prove the contrapositive. That is, if there is no clique of size  $k$  in  $G$ , then the reduced PAA instance is infeasible. We proceed by showing that there must be exactly  $k$  non-zero entries in the column vector  $\{s'_{i1} | i \leq n\}$  in order to satisfy constraints  $D_{\text{seq}}(S, S') \leq L = 6k$  and  $D_{\text{str}}(\mathcal{A}(S), \mathcal{A}(S')) \geq U$  and that, if there is no clique of size  $k$ , then there is no choice of  $k$  non-zero entries in  $\{s'_{i1} | i \leq n\}$  that will satisfy these constraints. Let  $k'$  denote the number of non-zero entries in  $\{s'_{i1} | i \leq n\}$ . To satisfy  $D_{\text{seq}}(S, S') \leq L = 6k$ , it follows that  $k' \leq k$ . If  $k' < k$ , then the maximum value of  $D_{\text{str}}(\mathcal{A}(S), \mathcal{A}(S'))$  is  $\frac{k'(k'-1)}{2} \sqrt{\frac{3}{n}} < \frac{k(k-1)}{2} \sqrt{\frac{3}{n}}$  and denotes to the case where the  $k'$  non-zero entries correspond to a clique of size  $k'$  in  $G$ . The strict inequality is due to the monotonically increasing nature of this equation. Therefore, it must be that  $k = k'$  and we have outputs  $x'_1 = y'_1 = z'_1 = k(k-1)/2$  as before. Suppose that the  $k'$  non-zero entries in  $\{s'_{i1} | i \leq n\}$  do not correspond to a clique in  $G$ . Then the values  $x'_1, y'_1,$  and  $z'_1$  output by  $\mathcal{A}$  and corresponding to the number of edges induced by the chosen non-zero entries would be strictly less than  $k(k-1)/2$ . Therefore, we would have  $D_{\text{str}}(\mathcal{A}(S), \mathcal{A}(S')) < U$ . This proves that the reduced PAA is infeasible.  $\square$

Table 1: RMSD results when  $L \in \{20, 30, 40\}$ .

Seq. ID	$n$	$L$	RMSD	$\mu_{\text{all}}$	$\mu_{\text{diff}}$	$\mu'_{\text{all}}$	$\mu'_{\text{diff}}$
Q14653	427	20	18.87	79.76	92.92	79.46	86.29
Q14653	427	30	22.42	79.76	93.15	77.45	64.12
Q14653	427	40	28.28	79.76	90.49	79.42	69.026
Q5BJD5	291	20	14.311	82.23	89.77	80.6	80.64
Q5BJD5	291	30	15.708	82.23	59.26	83.13	43.53
Q5BJD5	291	40	17.132	82.23	62.02	83.21	62.83
P59595	422	20	24.321	68.25	91.44	67.05	89.51
P59595	422	30	30.139	68.25	93.142	67.44	89.29
P59595	422	40	30.675	68.25	46.87	66.4	29.33
PODTC9	419	20	26.51	68.39	80.32	68.09	80.316
PODTC9	419	30	26.27	68.39	68.05	68.61	65.18
PODTC9	419	40	31.33	68.39	40.52	67.76	35.56
P07711	333	20	7.09	93.68	92.4	93.2	81.12
P07711	333	30	8.52	93.68	95.91	92.95	92.69
P07711	333	40	9.246	93.68	95.91	92.85	95.76
Q9Y397	364	20	11.184	84.24	97.35	83.85	95.81
Q9Y397	364	30	11.828	84.24	95.91	83.51	85.416
Q9Y397	364	40	14.222	84.24	95.91	83.71	89.79

Table 2: RMSD results for the three considered categories.

Seq. ID	$n$	Category	RMSD	$\mu_{\text{all}}$	$\mu_{\text{diff}}$	$\mu'_{\text{all}}$	$\mu'_{\text{diff}}$
Q01629	132	MIN.	6.02	64.63	32.44	60.99	36.99
Q01629	132	AVG.	19.92	64.63	64.75	63.77	69.57
Q01629	132	MAX.	19.906	64.63	66.99	90.21	90.19
Q5BJD5	291	MIN.	14.023	82.23	38.86	81.22	37.79
Q5BJD5	291	AVG.	14.232	82.23	82.24	81.17	77.23
Q5BJD5	291	MAX.	13.567	82.23	98.17	82.42	98.1
P59595	422	MIN.	24.74	68.25	29.13	67.57	31.5
P59595	422	AVG.	28.164	68.25	69.44	68.69	69.04
P59595	422	MAX.	24.62	68.25	96.14	67.51	96.44
P59633	154	MIN.	21.67	44.82	27.14	44.15	38.75
P59633	154	AVG.	21.52	44.82	45.1	43.8	42.26
P59633	154	MAX.	23.13	44.82	61.26	46.13	54.84
PODTC9	419	MIN.	25.593	68.39	28.46	67.9	28.83
PODTC9	419	AVG.	21.767	68.39	68.37	68.5	70.83
PODTC9	419	MAX.	23.685	68.39	97.1	68.64	96.94

## Experimental Results

For our experimental setup, we use the default settings of the latest version of AlphaFold <sup>1</sup>. This includes the initial multi-sequence alignment (MSA) step, the five-model ensembles predictions, recycling, output confidence ranking, and amber relaxation. For further details about each step, we refer the reader to (Jumper et al. 2021a) and its supplementary information. We include results from using the high-accuracy full database configuration of the initial AlphaFold MSA step along with the less accurate (and faster) reduced database option. In order to compute the RMSD and GDT, we need to employ an alignment algorithm. In this paper, we use the built-in alignment PyMOL procedure without outlier rejections (Schrödinger and DeLano). The parameters of PyMOL alignment are selected using the default settings, which include an outlier rejection cutoff of 2, a maximum number of outlier rejection cycles of 5, and the use of the structural superposition step. We note that these outliers only impact the calculations of the RMSD.

Our adversarial sequences are generated by randomly sampling 20 sequences from the set  $\mathcal{V}_{L,H}$  in (5) with  $H = 5$  and  $L = 20$ . Then, we pick the sequence that returns the maximum value in RMSD structural distance. We use an

<sup>1</sup><https://github.com/deepmind/alphafold>

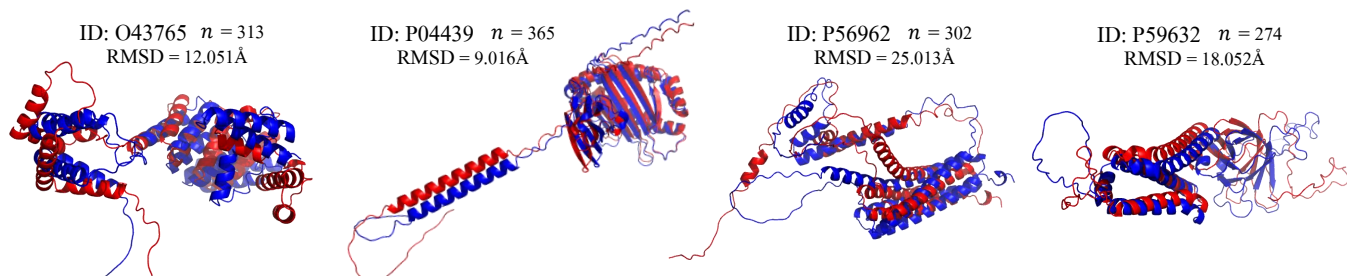


Figure 4: The structures of the original (black) and adversarial (red) sequences from AlphaFold. The 3D plots, aligned using PyMol (Schrödinger and DeLano), are for proteins O43765 (first), P04439 (second), P56962 (third), and P59632 (fourth). For structure differences, the RMSD values are reported. The structures of the complete list of sequences are given in the supplementary material.

Table 3: RMSD, GDT-TS, and GDT-HA results using the full database AlphaFold configuration with  $L = 20$  and  $H = 5$ . The average columns correspond to 20 adversarial samples for each protein ID. The complete table is placed in the supplementary material.

Seq. ID	$n$	Similarity (%)	RMSD	Avg. RMSD	GDT-TS (%)	Avg. GDT-TS (%)	GDT-HA (%)	Avg. GDT-HA (%)	run-time (days)
O43765	313	98.4026	14.438	9.1741	13.9776	35.4832	2.8754	17.6358	1.6068
P56962	302	98.3444	22.301	15.8695	12.3344	18.6921	3.4768	5.803	0.5959
P04439	365	98.6301	6.162	3.7942	47.7397	68.2705	25.0	45.774	0.6429
Q99836	296	98.3108	8.761	5.2907	24.1554	46.6723	7.6858	26.2584	0.6246
P59632	274	98.1752	13.018	8.4704	24.8175	41.0401	9.0328	21.6834	0.5214

AMD EPYC 7702 64-Core Processor with 1 TiB of RAM and NVIDIA A100 GPU. We generate adversarial sequences against the COVID-19 protein sequences from the UniProt database considered by AlphaFold in (Jumper et al. 2020). The original fasta (file extension for protein sequences) sequence files are available online <sup>2</sup>. Additionally, we generate adversarial sequences against most of the the UniProt (Universal Protein resource, a central repository of protein data created by combining the Swiss-Prot, TrEMBL and PIR-PSD databases (uni 2021)). Our code is provided as supplementary material.

### BLOSUM Threshold Experiment

In this subsection, we want to investigate how a change in the bound on biological similarity changes the adversarial sequence. In other words, we show the impact of using different BLOSUM thresholds in set  $\mathcal{V}_{L,H}$ . As such, we randomly select 6 sequences and generate adversarial sequences by configuring the BLOSUM threshold,  $L$ , to be 20, 30, and 40 (we use strict equalities to ensure the exact BLOSUM distance) and set  $H = 5$ . For each case, we obtain the RMSD after alignment as reported in the fourth column of Table 1. Furthermore, we present the average confidence percentage level of the prediction of the original (adversarial) sequence as reported by AlphaFold and denoted by  $\mu_{\text{all}}$  ( $\mu'_{\text{all}}$ ). Additionally, in the 6th and 8th columns, we report the average confidence values for the residues that are different between the original and adversarial sequences. These are denoted by  $\mu_{\text{diff}}$  and  $\mu'_{\text{diff}}$ , respectively. We observe that, in general, when the BLOSUM threshold distance increases, the RMSD also increases. This means that biologically increased distance in the input space, in general, causes higher changes in the output predictions of AlphaFold. In terms of the confidence scores, we observe that the change in the overall average confidence between the original and perturbed sequence is not

significant. However, in almost all the considered cases, we notice that the prediction confidence of the altered residues has reduced for the adversarial sequence when compared to the ones reported for the original sequence.

### Confidence Experiment

Given a sequence  $S$ , per residue, AlphaFold generates an estimate of its prediction confidence in the form of a value in  $[0, 100]$ . This value is called the predicted Local Distance Test (pLDDT) and represents the predicted value on the IDDT-C $\alpha$  metric (Mariani et al. 2013).

In this subsection, we answer the following question. Does selecting the residues to be changed based on their low (or high) confidence scores impact the resulting RMSD between the original and adversarial structure prediction? Phrased differently, in terms of the RMSD, we illustrate the impact of using the prediction confidence scores of every residue of the predicted structure of the original sequence in determining the location of the residues to be altered in the adversarial sequence generation method presented in the previous section. As such, five, not cherry picked, randomly selected sequences are used. Then, the locations of the 5 residues to be altered are taken based on three categories as follows. Residues are selected with confidence values near the (i) minimum confidence score (MIN. category), (ii) the average score (AVG. category), and (iii) the maximum confidence score (MAX. category). Results are presented in Table 2. We observe that, in general, selecting residues with low or high confidence scores is not related to the amount of the induced RMSD at the output. As such, in our method, the locations of the flipped residues are selected independent of the confidence scores.

### COVID-19 Case Studies

We apply our adversarial approach to 111 publicly available COVID-19 protein sequences as of the time of this writing per the UniProt database using AlphaFold full database configuration. Additionally, in the supplementary material, we

<sup>2</sup>[https://ftp.uniprot.org/pub/databases/uniprot/pre\\_release/covid-19.fasta](https://ftp.uniprot.org/pub/databases/uniprot/pre_release/covid-19.fasta)

Table 4: Prediction confidence results using the full database AlphaFold configuration with  $L = 20$ .

Seq. ID	$n$	RMSD	$\mu_{\text{all}}$	$\sigma_{\text{all}}$	$\mu_{\text{diff}}$	$\sigma_{\text{diff}}$	$\mu'_{\text{all}}$	$\sigma'_{\text{all}}$	$\mu'_{\text{diff}}$	$\sigma'_{\text{diff}}$
O43765	313	14.438	80.221	19.634	94.786	1.027	80.554	19.423	93.71	1.392
P56962	302	22.301	69.172	23.753	96.516	0.409	69.342	23.759	96.54	0.463
P04439	365	6.162	86.845	18.995	44.23	2.704	86.921	19.068	44.678	3.968
Q99836	296	8.761	81.213	13.817	78.914	7.454	80.918	13.971	72.198	6.253
P59632	274	13.018	58.367	18.783	66.136	2.029	57.364	18.794	60.926	4.362

Table 5: Overall Prediction and attack results for the reduced and full database configurations of AlphaFold.

Configuration.	Avg. $n$	Std. $n$	Avg. $\mu_{\text{all}}$	Std. $\mu_{\text{all}}$	Avg. RMSD	Std. RMSD	Avg. GDT	Std. GDT	Avg. run-time	Std. run-time
reduced database	480.53	416.66	78.22	10.96	15.31	11.24	34.08	28.39	0.68	0.59
full database	410.73	336.63	78.25	10.23	14.78	11.18	34.95	28.16	0.86	0.63

provide complete results using the reduced AlphaFold configuration. The BLOSUM62 distance between the original and adversarial sequences is at most 20, thus they are biologically close to each other (Chothia and Lesk 1986; Sander and Schneider 1991). Given the long list of the considered sequences, we describe only the following. SGTA\_HUMAN Small glutamine-rich tetratricopeptide repeat-containing protein alpha (O43765), HLA\_HUMAN HLA class I histocompatibility antigen, A alpha chain (P04439), STX17\_HUMAN Syntaxin-17 (P56962), AP3A\_SARS ORF3a (P59632), and MYD88\_HUMAN Myeloid differentiation primary response protein MyD88 (Q99836). The cases covered include homo sapiens and severe acute respiratory syndrome coronavirus 2 (2019-nCoV) (SARS-CoV-2) organisms which provide a wide variety of proteins. The considered sequences vary in length as they range from  $n = 22$  to  $n = 2511$ .

Figures 1 and 4 show the aligned predicted structures of the proteins described earlier where the original sequence is given in black and the adversarial sequence is given in red. We observe that, independent of the predicted structure of the original sequence, a small change in the input sequence results in significant changes in the output structures. The resulting structural distances (similarities) measured in Å (percentage) are given in terms of the RMSD (GDT-TS) in the fourth (sixth) column of Table 9 for the full database configuration. Furthermore, we report the results using GDT-HA in the eighth column. The high similarity between the original and adversarial sequences is observed from the third column. The similarity percentage is calculated as  $100(n - D_{\text{ham}}(S, S'))/n$ , where  $D_{\text{ham}}(S, S') \leq H = 5$ . The complete results of all the considered proteins, including reduced AlphaFold configuration, are provided in the supplementary material.

As observed from the RMSD and GDT results in Table 9, small changes in the input sequence corresponding to only five residues cause AlphaFold to predict structures that are highly divergent from the predicted structure of the original sequence. The last column in Table 9 reports the total execution time (in days) of running the 20 adversarial sequences that were randomly selected from the set  $\mathcal{V}_{L,H}$ , which is shown to scale with the sequence length. We only select 20 samples given the long time incurred by AlphaFold to predict the output structure.

Additionally, in Table 13, we report the average (deviation) prediction confidence results as for all the residues (designated with subscript ‘all’) and for the 5 altered residues (subscript ‘diff’). The standard deviation is denoted  $\sigma$ . We ob-

serve that, independent of the average prediction confidence, the RMSD between the original and adversarial predicted structures is always high. This is noted for both the full and reduced database configurations of AlphaFold. Moreover, we observe that AlphaFold predicts the adversarial structure with similar confidence values to the original sequence (e.g., see the 4th and 8th columns in both tables). The same observation holds for the entire sequence and for the altered residues (columns 6 and 10).

In Tables 14 and 15 of the supplementary, we break down GDT scores between the structures of the original and perturbed sequences based on the prediction confidence scores of the original sequence. We use the regions (1 to 4) defined by AlphaFold. As observed w.r.t. all regions, GDT scores are, in general, low.

For the considered dataset, the values presented in Table 5 gauge the overall robustness of AlphaFold to adversarial sequences. As indicated in the documentation of AlphaFold, for better accuracy, the full database configuration incurs a higher execution time compared to the reduced database configuration. The reported average values of the RMSD and GDT-TS measures are 14.78Å and 37.95%, respectively. In CASP14 (year 2020), AlphaFold achieved a median GDT-TS score of 92.4%, and 88% of their predictions fall under RMSD = 4Å<sup>3</sup>. These results are obtained by comparing the predicted and ground truth structures. The CASP14 AlphaFold results underscore the significance of the values reported in Tables 9 and 5, as they show how small changes in the input sequences could damage the predictions (See columns 6 to 9 in Table 5). The key takeaway is that *AlphaFold is generally not robust even when a basic approach is used to generate perturbations of the input protein sequence.*

## Conclusion

The groundbreaking progress made in recent years on the prediction of protein folding structures promises to enable profound advances in the understanding of diseases, the mapping of the human proteome, and the design of drugs and therapeutics. However, until these predictions are shown to be robust, we argue that the grand challenge of predictive protein folding persists. In this paper, we have presented the first work in this direction by demonstrating that Protein Folding Neural Networks (PFNNs) are often susceptible to adversarial attacks in the form of minor perturbations to the input protein sequence. These perturbations can induce

<sup>3</sup><https://predictioncenter.org/casp14/index.cgi>

great changes in the predicted protein structure and the resulting lack of robustness precludes the adoption of such PFNNs in safety-critical applications. We have employed standard protein structural distance and similarity to measure the robustness of AlphaFold. While the perturbation methods employed in this paper were basic for the purposes of illustrating the lack of robustness of PFNNs, the results presented herein can be readily used as a baseline for future work on adversarial attacks on PFNNs and their robustness.

## References

2021. UniProt: the universal protein knowledgebase in 2021. *Nucleic acids research*, 49(D1): D480–D489.
- Andriushchenko, M.; Croce, F.; Flammarion, N.; and Hein, M. 2020. Square attack: a query-efficient black-box adversarial attack via random search. In *European Conference on Computer Vision*, 484–501. Springer.
- Baek, M.; DiMaio, F.; Anishchenko, I.; Dauparas, J.; Ovchinnikov, S.; Lee, G. R.; Wang, J.; Cong, Q.; Kinch, L. N.; Schaeffer, R. D.; et al. 2021. Accurate prediction of protein structures and interactions using a three-track neural network. *Science*, 373(6557): 871–876.
- Bagdonas, H.; Fogarty, C. A.; Fadda, E.; and Agirre, J. 2021. The case for post-predictional modifications in the AlphaFold Protein Structure Database. *Nature Structural & Molecular Biology*, 28(11): 869–870.
- Bai, Y.; Zeng, Y.; Jiang, Y.; Wang, Y.; Xia, S.-T.; and Guo, W. 2020. Improving query efficiency of black-box adversarial attack. In *Computer Vision—ECCV 2020: 16th European Conference, Glasgow, UK, August 23–28, 2020, Proceedings, Part XXV 16*, 101–116. Springer.
- Chan, H. S.; Shan, H.; Dahoun, T.; Vogel, H.; and Yuan, S. 2019. Advancing drug discovery via artificial intelligence. *Trends in pharmacological sciences*, 40(8): 592–604.
- Chothia, C.; and Lesk, A. M. 1986. The relation between the divergence of sequence and structure in proteins. *The EMBO journal*, 5(4): 823–826.
- Cordes, M. H. J.; Burton, R. E.; Walsh, N. P.; McKnight, C. J.; and Sauer, R. T. 2000. An evolutionary bridge to a new protein fold. *Nature Structural Biology*, 7(12): 1129–1132.
- Croce, F.; Andriushchenko, M.; Schwag, V.; Flammarion, N.; Chiang, M.; Mittal, P.; and Hein, M. 2020. Robustbench: a standardized adversarial robustness benchmark. *arXiv preprint arXiv:2010.09670*.
- Croce, F.; and Hein, M. 2021. Mind the box:  $l_1$ -APGD for sparse adversarial attacks on image classifiers. *arXiv preprint arXiv:2103.01208*.
- Dayhoff, M.; Schwartz, R.; and Orcutt, B. 1978. 22 a model of evolutionary change in proteins. *Atlas of protein sequence and structure*, 5: 345–352.
- Del Alamo, D.; Sala, D.; Mchaourab, H. S.; and Meiler, J. 2022. Sampling alternative conformational states of transporters and receptors with AlphaFold2. *Elife*, 11: e75751.
- Goodfellow, I.; McDaniel, P.; and Papernot, N. 2018. Making machine learning robust against adversarial inputs. *Communications of the ACM*, 61(7): 56–66.
- Henikoff, S.; and Henikoff, J. G. 1992. Amino acid substitution matrices from protein blocks. *Proceedings of the National Academy of Sciences*, 89(22): 10915–10919.
- Jha, S. K.; Ramanathan, A.; Ewetz, R.; Velasquez, A.; and Jha, S. 2021. Protein folding neural networks are not robust. *arXiv preprint arXiv:2109.04460*.
- Jones, D. T.; Taylor, W. R.; and Thornton, J. M. 1992. The rapid generation of mutation data matrices from protein sequences. *Bioinformatics*, 8(3): 275–282.
- Jumper, J.; Evans, R.; Pritzel, A.; Green, T.; Figurnov, M.; Ronneberger, O.; Tunyasuvunakool, K.; Bates, R.; Židek, A.; Potapenko, A.; Bridgland, A.; Meyer, C.; Kohl, S. A. A.; Ballard, A. J.; Cowie, A.; Romera-Paredes, B.; Nikolov, S.; Jain, R.; Adler, J.; Back, T.; Petersen, S.; Reiman, D.; Clancy, E.; Zielinski, M.; Steinegger, M.; Pacholska, M.; Berghammer, T.; Bodenstein, S.; Silver, D.; Vinyals, O.; Senior, A. W.; Kavukcuoglu, K.; Kohli, P.; and Hassabis, D. 2021a. Highly accurate protein structure prediction with AlphaFold. *Nature*, 596(7873): 583–589.
- Jumper, J.; Evans, R.; Pritzel, A.; Green, T.; Figurnov, M.; Ronneberger, O.; Tunyasuvunakool, K.; Bates, R.; Židek, A.; Potapenko, A.; et al. 2021b. Highly accurate protein structure prediction with AlphaFold. *Nature*, 596(7873): 583–589.
- Jumper, J.; Tunyasuvunakool, K.; Kohli, P.; Hassabis, D.; and Team, A. 2020. Computational predictions of protein structures associated with COVID-19. *DeepMind website*.
- Mahmood, K.; Mahmood, R.; Rathbun, E.; and Van Dijk, M. 2021. Back in Black: A Comparative Evaluation of Recent State-Of-The-Art Black-Box Attacks. *IEEE Access*.
- Mariani, V.; Biasini, M.; Barbato, A.; and Schwede, T. 2013. IDDT: a local superposition-free score for comparing protein structures and models using distance difference tests. *Bioinformatics*, 29(21): 2722–2728.
- Papernot, N.; McDaniel, P.; Goodfellow, I.; Jha, S.; Celik, Z. B.; and Swami, A. 2017. Practical black-box attacks against machine learning. In *ACCS'17*.
- Rost, B. 1999. Twilight zone of protein sequence alignments. *Protein engineering*, 12(2): 85–94.
- Sander, C.; and Schneider, R. 1991. Database of homology-derived protein structures and the structural meaning of sequence alignment. *Proteins: Structure, Function, and Bioinformatics*, 9(1): 56–68.
- Schrödinger, L.; and DeLano, W. P. PyMOL.
- Stein, R. A.; and Mchaourab, H. S. 2021. Modeling alternate conformations with alphafold2 via modification of the multiple sequence alignment. *bioRxiv*.
- Tuinstra, R. L.; Peterson, F. C.; Kutlesa, S.; Elgin, E. S.; Kron, M. A.; and Volkman, B. F. 2008. Interconversion between two unrelated protein folds in the lymphotactin native state. *Proceedings of the National Academy of Sciences*, 105(13): 5057–5062.
- Zemla, A. 2003. LGA: a method for finding 3D similarities in protein structures. *Nucleic acids research*, 31(13): 3370–3374.



Table 6: RMSD, GDT-TS, and GDT-HA results using the reduced database AlphaFold configuration with  $L = 20$  and  $H = 5$ . The average results correspond to 20 adversarial samples for each protein ID. Part I of II.

Protein ID	$n$	Similarity (%)	RMSD	Avg. RMSD	GDT-TS (%)	Avg. GDT-TS (%)	GDT-HA (%)	Avg. GDT-HA (%)	run-time (days)
A0A663	38	86.8421	3.129	1.655	78.9474	95.0	57.2368	84.5395	0.4173
MPROTEI	193	97.4093	2.06	1.2348	83.1606	97.0531	60.6218	89.6308	0.7081
NSP2NNN	546	99.0842	19.561	11.4867	4.2125	19.9657	0.3663	7.0696	1.6596
NSP4NNN	494	98.9879	11.389	2.9463	6.5789	72.7277	0.253	51.1943	1.6327
NSP6NNN	290	98.2759	8.921	3.5994	29.4828	79.7716	9.3966	62.7629	0.9444
O00327	626	99.2013	10.445	5.7079	26.3578	52.6637	9.6645	31.4177	0.5849
O14745	358	98.6034	12.34	8.3659	7.6117	24.7835	0.5587	8.6627	0.4956
O14786	923	99.4583	33.465	11.134	0.5688	45.6744	0.0271	27.1682	0.7755
O15393	492	98.9837	24.847	13.9194	6.7073	32.9014	1.1179	15.3938	0.5225
O15455	904	99.4469	24.886	11.3427	5.3927	33.4748	0.9403	17.1308	0.7941
O43765	313	98.4026	12.051	9.9661	17.0927	25.1917	2.7157	8.746	0.4918
O94826	608	99.1776	11.824	6.2432	50.6579	65.514	29.4819	44.4881	0.5685
O95721	258	98.062	8.478	4.6662	44.9612	70.063	24.9031	50.126	0.454
O95786	925	99.4595	33.92	21.8359	2.2432	20.2216	0.2162	11.9811	0.7688
O95992	272	98.1618	6.531	2.9731	52.9412	81.6636	29.5037	67.7482	0.4474
P00973	400	98.75	7.988	2.3463	47.4375	88.9125	24.4375	77.2094	0.4775
P01185	164	96.9512	5.552	3.1564	42.378	64.436	19.6646	40.3887	0.4217
P01889	362	98.6188	9.904	4.847	39.8481	64.0331	18.9227	41.5021	0.4832
P02649	317	98.4227	16.897	7.5644	17.0347	57.1017	0.4732	34.6845	0.4661
P04233	296	98.3108	17.217	9.0204	12.0777	38.7204	1.8581	18.4628	0.4549
P04439	365	98.6301	9.016	4.1563	35.8219	66.3493	14.4521	44.0616	0.4864
P05109	93	94.6237	1.953	1.6582	92.4731	94.5968	75.8065	81.1694	0.4072
P05161	165	96.9697	2.557	1.7111	80.1515	93.1364	57.2727	80.8864	0.4191
P05231	212	97.6415	7.214	4.1072	42.8066	60.513	22.2877	38.6321	0.4332
P07711	333	98.4985	8.263	1.985	38.964	92.0983	17.3423	78.9752	0.4595
P08887	468	98.9316	11.083	8.7031	26.1218	37.2409	10.5769	17.8846	0.4983
P09429	215	97.6744	24.633	16.3079	4.0698	24.1686	0.6977	12.4767	0.455
P09958	794	99.3703	24.603	10.7503	10.8627	35.2503	1.7947	17.7031	0.6753
PODTC2	1273	99.6072	10.44	3.0204	44.3048	88.9209	22.9772	74.8075	1.0189
PODTC3	275	98.1818	16.932	11.541	11.5455	32.6818	3.2727	15.25	0.4574
PODTC4	75	93.3333	3.403	2.3942	64.3333	79.0333	40.3333	56.5833	0.4234
PODTC5	222	97.7477	9.978	3.837	32.8829	82.2185	12.6126	63.7106	0.4534
PODTC6	61	91.8033	5.379	1.6014	54.0984	94.7131	29.918	84.6516	0.4095
PODTC7	121	95.8678	8.067	2.5574	28.5124	79.5971	9.2975	58.626	0.4249
PODTC8	121	95.8678	17.706	11.063	12.3967	36.6322	2.8926	20.7645	0.4237
PODTC9	419	98.8067	27.007	13.6089	6.1456	29.8896	1.4916	12.3628	0.4926
PODTD2	97	94.8454	4.388	2.318	65.9794	88.4665	43.299	72.8479	0.4032
PODTD3	73	93.1507	24.441	11.5174	2.3973	26.7466	0.0	11.4555	0.4123
PODTD8	43	88.3721	2.458	1.2823	86.6279	99.3023	68.0233	97.907	0.4048
PODTF1	22	77.2727	2.589	1.5475	81.8182	96.9886	61.3636	89.8864	0.4074
PODTG0	57	91.2281	12.352	9.0543	15.3509	38.7939	3.0702	18.2018	0.402
PODTG1	41	87.8049	15.533	7.8958	10.3659	49.2073	1.2195	30.5488	0.413
P11226	248	97.9839	16.516	10.4097	13.5081	29.9899	1.5121	12.6562	0.451
P13164	125	96.0	30.581	9.2107	4.4	32.51	0.6	13.72	0.4133
P13747	358	98.6034	14.9	9.3546	25.0	42.6082	6.6341	21.1278	0.48
P17181	557	99.1023	12.674	7.6171	29.4883	49.8564	11.5799	29.5781	0.5437
P17405	631	99.2076	12.182	5.0017	55.9826	72.6743	32.9239	52.4148	0.5852
P20701	1170	99.5726	10.129	4.6012	41.1752	77.5224	20.0641	59.2447	1.0466
P26022	381	98.6877	15.865	12.3077	13.5171	25.6135	2.4278	9.9278	0.5793
P26715	233	97.8541	30.415	14.0567	0.4292	23.7124	0.0	9.0397	0.4332
P29597	1187	99.5788	5.571	3.6236	81.4659	92.2315	61.8576	78.7584	1.176
P30556	359	98.6072	12.313	8.9116	19.8468	47.4861	6.1281	27.4617	0.4759
P33076	1130	99.5575	30.469	15.9168	11.5487	35.9104	1.8584	17.4569	0.9424
P35232	272	98.1618	2.652	2.018	68.8419	83.0101	44.6691	62.5322	0.4467
P35613	385	98.7013	9.773	3.5793	30.0649	73.2597	9.7403	51.5844	0.4875
P40189	918	99.4553	22.039	14.3382	32.7342	46.8301	13.1808	27.5844	0.7851
P47901	424	98.8208	17.192	6.5205	19.2807	61.1468	3.6557	40.9788	0.4898
P48551	515	99.0291	36.573	22.2727	3.1553	12.7184	0.2427	3.2985	0.5227
P49327	2511	99.8009	33.768	21.222	4.5301	25.6004	0.0299	14.4922	4.7273
P49754	854	99.4145	6.766	3.607	49.678	64.7263	26.171	40.7172	1.4149
P51149	207	97.5845	7.341	3.9087	34.6618	62.7355	13.7681	40.0	0.4462

Table 7: RMSD, GDT-TS, and GDT-HA results using the reduced database AlphaFold configuration with  $L = 20$  and  $H = 5$ . The average results correspond to 20 adversarial samples for each protein ID. Part II of II.

Protein ID	$n$	Similarity (%)	RMSD	Avg. RMSD	GDT-TS (%)	Avg. GDT-TS (%)	GDT-HA (%)	Avg. GDT-HA (%)	run-time (days)
P52292	529	99.0548	9.065	4.3164	44.9433	75.0071	23.3459	54.5723	0.531
P52948	1817	99.7248	56.34	39.782	1.9125	8.2327	0.0413	2.4869	2.0914
P56962	302	98.3444	25.013	19.3739	10.3477	18.0505	0.4139	5.1283	0.5233
P59594	1255	99.6016	4.432	2.9699	81.1355	88.4303	59.6016	72.8357	0.9841
P59595	422	98.8152	26.286	18.0807	4.0284	15.0474	0.7109	3.2524	0.4821
P59596	221	97.7376	9.173	4.2628	30.3167	71.1369	10.0679	55.6618	0.4292
P59632	274	98.1752	18.052	14.8883	9.854	21.3777	1.2774	7.6505	0.452
P59633	154	96.7532	20.183	12.9835	6.3312	22.8247	0.487	8.4253	0.4349
P59634	63	92.0635	2.5	1.8276	74.2063	86.2103	49.2063	64.8214	0.3953
P59635	122	95.9016	5.955	3.2856	56.3525	76.2807	32.582	54.0984	0.4216
P59636	98	94.898	3.095	1.6404	74.7449	92.8061	50.0	82.3469	0.4042
P59637	76	93.4211	1.743	1.4686	88.8158	94.7039	69.0789	78.5362	0.398
P62937	165	96.9697	1.011	0.9256	98.7879	99.9015	95.1515	98.6364	0.4252
P68104	462	98.9177	1.511	1.1407	92.316	98.0168	75.0	90.4654	0.58
P84022	425	98.8235	20.077	10.981	20.8235	42.6265	4.2941	21.6882	0.4813
PLRPOCT	355	98.5915	3.898	1.7713	68.0282	87.743	45.7042	69.6655	1.1182
Q01628	133	96.2406	21.561	9.1364	5.2632	35.4323	0.7519	18.5526	0.4171
Q01629	132	96.2121	12.883	6.0595	20.0758	47.9451	3.7879	26.8182	0.4109
Q10589	180	97.2222	2.608	1.821	72.9167	84.7986	50.0	65.3264	0.4185
Q13241	179	97.2067	7.989	4.4141	27.514	57.6676	9.3575	34.4553	0.4268
Q13568	498	98.996	21.258	12.6381	3.4137	22.623	0.251	8.2204	0.5214
Q14653	427	98.829	20.062	10.4706	5.2108	28.9754	1.1124	16.1036	0.4917
Q16236	605	99.1736	30.752	16.7302	4.2562	19.7355	0.2893	6.9855	0.5603
Q16552	155	96.7742	17.781	3.333	7.0968	76.5081	1.2903	57.7177	0.4254
Q16553	131	96.1832	13.654	9.6988	26.5267	40.4294	10.1145	21.7557	0.4112
Q16665	826	99.3947	44.207	36.917	2.0278	7.3229	0.1816	1.6525	0.9057
Q4KMQ2	910	99.4505	2.872	1.5488	88.544	96.1607	70.2198	91.5618	0.9261
Q5BJD5	291	98.2818	14.524	8.7746	24.7423	50.5241	4.2955	29.3084	0.5373
Q5W0Z9	365	98.6301	21.394	9.5701	12.0548	49.089	3.1507	30.2158	0.4627
Q7TFA0	39	87.1795	14.095	4.5293	13.4615	63.9103	1.9231	41.9872	0.4068
Q7TFA1	44	88.6364	2.214	1.5401	93.75	97.1023	78.9773	89.858	0.3947
Q7TLC7	70	92.8571	24.421	17.726	2.8571	8.9643	0.0	2.1607	0.401
Q7Z434	540	99.0741	49.531	37.777	5.463	9.3356	0.787	3.2292	0.9567
Q80H93	84	94.0476	16.513	10.7184	16.6667	29.5089	3.2738	10.6994	0.4066
Q86U44	580	99.1379	21.605	15.7778	7.2414	17.4806	1.4655	5.4095	0.5432
Q86WV6	379	98.6807	18.481	6.0665	32.2559	75.752	15.6332	58.6642	0.4831
Q8IUC6	712	99.2978	28.425	22.4454	5.3722	15.2809	0.5267	5.2107	0.6707
Q8N3R9	675	99.2593	31.253	12.4049	2.5185	31.8722	0.2593	15.6926	0.6038
Q8N884	522	99.0421	22.258	12.97	16.092	40.6106	4.3582	21.9732	0.538
Q8NAC3	791	99.3679	11.777	10.0046	34.9558	44.5765	16.024	23.8827	0.6844
Q8NEB9	887	99.4363	21.53	7.738	9.4983	53.0116	1.0428	36.4402	0.8231
Q8NHX9	752	99.3351	7.509	2.9775	59.9734	86.9016	35.8378	75.3059	0.6296
Q92499	740	99.3243	9.308	4.487	30.8784	61.1909	12.7703	39.375	0.6791
Q92985	503	99.006	26.943	9.5613	4.9205	37.9796	0.994	18.1337	0.5065
Q96C10	678	99.2625	2.133	1.4139	90.1917	96.5874	72.4926	87.5406	0.6076
Q96F46	866	99.4226	42.175	31.9609	2.1363	4.4284	0.1443	0.8213	0.7225
Q96JC1	886	99.4357	2.853	1.5242	68.4819	91.2091	43.9616	77.7963	0.7552
Q96PD0	1036	99.5174	12.888	5.9922	13.7307	55.7384	3.8369	36.11	0.986
Q96PD4	163	96.9325	14.017	4.404	27.1472	72.1779	7.5153	56.227	0.4585
Q99623	299	98.3278	8.752	4.3578	36.1204	56.8562	14.2977	34.4523	0.4998
Q99836	296	98.3108	6.525	4.4038	31.8412	49.6833	11.7399	26.7314	0.4677
Q9BV40	100	95.0	3.427	2.0524	60.75	82.1125	37.25	68.025	0.4523
Q9BYF1	480	98.9583	5.509	1.9196	65.6771	92.0182	41.875	76.8854	0.4854
Q9BYX4	1025	99.5122	4.818	3.6154	42.7317	57.2427	19.2439	33.9329	1.1546
Q9C000	1473	99.6606	35.861	17.441	2.6986	25.5431	0.3904	10.5821	1.398
Q9H074	479	98.9562	30.3	19.6118	6.524	19.6425	0.8351	7.8314	0.5462
Q9NR97	1041	99.5197	21.869	8.5147	5.3074	41.9681	1.2248	24.9412	1.0298
Q9NRS4	437	98.8558	6.233	3.0814	53.833	79.7368	29.7483	61.4045	0.5264
Q9NVJ2	186	97.3118	1.945	1.2634	88.4409	97.0027	68.9516	90.4368	0.4276
Q9NYK1	1049	99.5234	12.803	7.1807	25.9771	46.2345	6.9828	25.8115	1.0763
Q9UHD2	729	99.3141	5.063	2.4523	73.5597	92.3525	50.5487	83.5391	0.7376
Q9ULC8	765	99.3464	34.128	26.1615	5.1961	15.9297	1.3725	6.2614	0.8275
Q9Y2I7	2098	99.7617	34.987	27.8546	8.9967	22.4285	0.9771	9.4948	4.8776
Q9Y397	364	98.6264	11.551	6.3126	40.4533	65.783	19.7802	48.2521	0.4675

Table 8: RMSD, GDT-TS, and GDT-HA results using the full database AlphaFold configuration with  $L = 20$  and  $H = 5$ . The average results correspond to 20 adversarial samples for each protein ID. Part I of II.

Seq. ID	$n$	Similarity (%)	RMSD	Avg. RMSD	GDT-TS (%)	Avg. GDT-TS (%)	GDT-HA (%)	Avg. GDT-HA (%)	run-time (days)
A0A663	38	86.8421	2.886	1.7076	82.8947	95.0	63.8158	85.7566	0.4058
MPROTEI	193	97.4093	5.562	4.8324	37.5648	45.2785	13.4715	23.1995	0.5288
NSP2NNN	546	99.0842	22.333	8.7108	8.3791	33.6332	1.3736	16.0119	0.885
NSP4NNN	494	98.9879	16.995	14.4184	7.2368	13.4261	1.0121	2.9681	0.6312
NSP6NNN	290	98.2759	5.41	3.2315	66.4655	85.2543	42.931	67.944	0.5433
O00327	626	99.2013	18.69	5.133	10.1438	62.7456	0.7188	41.1621	1.8352
O14745	358	98.6034	7.395	3.6869	23.3939	57.2521	4.8184	33.7919	0.8124
O14786	923	99.4583	36.546	17.6305	1.0022	31.0455	0.0271	16.2649	1.4629
O15393	492	98.9837	19.978	13.4431	9.4512	33.5823	2.6423	15.0737	0.8496
O15455	904	99.4469	20.539	8.6482	8.4071	39.6391	1.3551	20.0733	2.2111
O43765	313	98.4026	14.438	9.1741	13.9776	35.4832	2.8754	17.6358	1.6068
O94826	608	99.1776	8.407	5.513	48.7253	70.4996	27.426	52.021	2.4019
O95721	258	98.062	11.099	4.2622	32.2674	69.6754	11.8217	49.4234	0.5642
O95992	272	98.1618	5.988	3.0947	54.3199	79.5864	31.1581	64.3244	0.5627
P00973	400	98.75	14.825	7.3132	24.0625	52.4594	6.9375	30.7406	0.6362
P01185	164	96.9512	7.641	3.0531	32.4695	67.4085	10.8232	43.628	0.4879
P01889	362	98.6188	9.441	5.624	40.5387	58.7017	19.4061	36.5608	0.638
P02649	317	98.4227	22.675	13.6351	2.3659	24.1916	0.0789	11.455	0.6008
P04233	296	98.3108	18.279	7.6704	15.625	39.9535	2.2804	18.6529	0.5748
P04439	365	98.6301	6.162	3.7942	47.7397	68.2705	25.0	45.774	0.6429
P05109	93	94.6237	1.19	0.9509	96.2366	98.9247	92.4731	96.707	0.4963
P05161	165	96.9697	2.569	1.2816	80.6061	96.4621	57.8788	90.3485	0.5225
P05231	212	97.6415	9.402	3.6258	28.8915	64.7642	9.7877	42.8715	0.5111
P07711	333	98.4985	7.479	1.6907	44.0691	93.0856	21.1712	82.9467	0.6467
P08887	468	98.9316	10.171	6.0542	36.3782	50.86	15.812	29.3109	0.8998
P09429	215	97.6744	20.391	12.9117	7.6744	26.4767	1.2791	10.6628	0.5901
P09958	794	99.3703	32.057	17.4892	4.8489	22.9455	0.3778	9.3923	1.5547
PODTC2	1273	99.6072	4.917	3.6252	81.1076	88.0027	60.546	71.8274	1.5762
PODTC3	275	98.1818	11.391	7.6561	28.9091	47.5182	11.6364	27.0682	0.5612
PODTC4	75	93.3333	2.496	1.4206	73.6667	92.8667	51.0	77.7667	0.4491
PODTC5	222	97.7477	6.436	1.9211	67.2297	91.9032	46.7342	81.6667	0.5269
PODTC6	61	91.8033	4.88	1.547	56.9672	95.4508	33.1967	85.6352	0.4218
PODTC7	121	95.8678	4.492	2.8855	53.719	77.0558	30.1653	55.0103	0.4462
PODTC8	121	95.8678	17.601	12.2174	11.5702	25.9194	2.4793	9.6798	0.4668
PODTC9	419	98.8067	29.977	18.2825	3.58	17.148	0.358	6.8377	0.604
PODTD2	97	94.8454	4.156	2.0488	65.9794	89.884	42.268	74.9485	0.439
PODTD3	73	93.1507	17.276	12.5488	3.7671	16.2671	0.0	3.8699	0.4229
PODTD8	43	88.3721	2.394	1.2436	90.1163	99.4477	73.8372	97.936	0.4274
PODTF1	22	77.2727	2.033	1.5082	86.3636	97.6136	64.7727	90.3409	0.4111
PODTG0	57	91.2281	13.398	7.9086	17.1053	43.9693	3.5088	23.8596	0.4064
PODTG1	41	87.8049	17.037	8.2412	7.3171	45.8537	0.6098	28.811	0.4122
P11226	248	97.9839	21.819	10.5974	8.871	31.744	0.6048	14.7782	0.6851
P13164	125	96.0	8.675	3.759	30.2	69.17	10.8	47.44	0.4743
P13747	358	98.6034	12.178	9.1998	27.8631	42.6013	8.8687	22.8631	0.6393
P17181	557	99.1023	21.61	15.1002	16.3375	30.7989	5.0718	13.8353	1.1425
P17405	631	99.2076	12.066	4.2296	52.6149	75.9311	29.8336	56.6442	0.9839
P20701	1170	99.5726	8.323	4.1428	34.9786	62.5865	12.3504	39.1603	2.4989
P26022	381	98.6877	14.411	9.0528	18.2415	41.9029	4.3963	23.5138	0.949
P26715	233	97.8541	22.384	10.099	12.2318	35.0215	2.1459	16.0193	0.5796
P29597	1187	99.5788	32.804	22.2887	3.4751	31.9482	0.5897	20.8888	3.6416
P30556	359	98.6072	10.111	5.7957	23.6769	61.3962	8.2173	40.3343	0.6767
P33076	1130	99.5575	26.719	20.1579	13.6504	26.344	0.4646	10.1427	2.2339
P35232	272	98.1618	3.447	1.6141	63.2353	91.5074	39.4301	78.4559	0.5927
P35613	385	98.7013	8.896	3.4822	27.2078	68.9123	7.5325	46.8344	1.032
P40189	918	99.4553	24.632	10.274	27.9139	50.4112	11.7647	30.6727	2.0398
P47901	424	98.8208	5.702	3.889	49.8821	71.8013	28.3019	51.418	0.7334
P48551	515	99.0291	28.717	14.5889	4.9029	19.2087	0.0485	6.4102	0.7453
P51149	207	97.5845	6.188	2.8336	37.8019	80.8092	15.2174	61.3285	0.5977

Table 9: RMSD, GDT-TS, and GDT-HA results using the full database AlphaFold configuration with  $L = 20$  and  $H = 5$ . The average results correspond to 20 adversarial samples for each protein ID. This is part II of II.

Seq. ID	$n$	Similarity (%)	RMSD	Avg. RMSD	GDT-TS (%)	Avg. GDT-TS (%)	GDT-HA (%)	Avg. GDT-HA (%)	run-time (days)
P56962	302	98.3444	22.301	15.8695	12.3344	18.6921	3.4768	5.803	0.5959
P59596	221	97.7376	7.506	2.1014	33.9367	90.1923	11.7647	79.2251	0.5245
P59632	274	98.1752	13.018	8.4704	24.8175	41.0401	9.0328	21.6834	0.5214
P59633	154	96.7532	20.993	15.7533	5.3571	15.7468	0.3247	4.3912	0.4625
P59634	63	92.0635	2.514	1.5476	82.1429	94.3849	58.7302	77.619	0.4214
P59635	122	95.9016	6.527	4.9216	37.7049	58.4016	14.3443	34.7746	0.4458
P59636	98	94.898	5.647	1.8721	47.7041	89.3622	24.4898	78.3673	0.4361
P59637	76	93.4211	3.488	1.6534	64.1447	88.6513	40.4605	70.5592	0.4352
P62937	165	96.9697	0.963	0.8934	99.5455	99.947	97.1212	98.8333	0.5403
P68104	462	98.9177	1.547	1.3632	93.1818	96.1607	75.974	85.1677	0.8504
P84022	425	98.8235	16.633	7.2522	15.4706	52.5882	3.4706	31.4382	0.67
PLRPOCT	355	98.5915	3.824	1.4276	75.7746	93.4648	53.662	78.5493	0.5569
Q01628	133	96.2406	26.947	15.7051	3.0075	21.8797	0.3759	9.2011	0.498
Q01629	132	96.2121	18.508	10.094	16.0985	32.3201	4.1667	15.322	0.4848
Q10589	180	97.2222	11.884	3.1079	11.8056	73.3403	0.9722	53.7847	0.5251
Q13241	179	97.2067	11.456	5.3773	23.4637	50.4958	6.8436	28.9874	0.5468
Q13568	498	98.996	29.991	17.9838	1.2048	13.637	0.1004	5.1657	0.7167
Q14653	427	98.829	16.703	9.6337	15.0468	28.0884	3.9227	11.1797	0.6629
Q16236	605	99.1736	38.828	18.9672	4.5455	22.1591	0.0826	9.7376	0.8244
Q16552	155	96.7742	13.575	8.3168	17.4194	30.0242	3.5484	12.7823	0.4973
Q16553	131	96.1832	10.901	5.9358	46.7557	64.9523	28.4351	46.3836	0.4789
Q16665	826	99.3947	41.354	31.4424	5.9322	14.3644	0.4843	4.3614	2.0399
Q4KMQ2	910	99.4505	4.59	2.1627	83.022	94.5618	62.6374	87.2802	1.1123
Q5BJD5	291	98.2818	13.792	9.6387	27.6632	44.4674	7.5601	24.317	0.6327
Q5W0Z9	365	98.6301	15.887	6.2479	22.3288	63.8938	7.1918	42.9863	0.6469
Q7TFA0	39	87.1795	2.505	1.6814	87.8205	94.7115	66.6667	82.8205	0.4365
Q7TFA1	44	88.6364	2.106	1.552	94.8864	97.358	80.1136	90.5114	0.4189
Q7TLC7	70	92.8571	24.995	6.955	2.1429	54.0893	0.0	35.9464	0.4291
Q7Z434	540	99.0741	50.815	34.506	3.4722	8.9236	0.5093	2.8449	0.7655
Q80H93	84	94.0476	14.707	2.8159	17.8571	82.2173	3.2738	63.6012	0.446
Q86U44	580	99.1379	17.742	12.9209	22.2414	40.4203	4.8707	19.8448	0.7916
Q86WV6	379	98.6807	20.858	8.6755	11.9393	65.4617	3.628	53.5026	0.6223
Q8IUC6	712	99.2978	49.827	26.3508	0.6671	11.1464	0.0351	2.8002	0.813
Q8N3R9	675	99.2593	35.139	15.0821	4.4815	29.0204	0.7037	13.45	0.9995
Q8N884	522	99.0421	29.73	20.0914	7.6149	16.2883	1.5805	4.9449	0.7615
Q8NAC3	791	99.3679	11.202	7.0906	29.3616	49.9621	10.9039	27.9772	0.98
Q8NHX9	752	99.3351	6.888	5.0382	56.9149	72.9887	32.879	52.387	1.1902
Q92499	740	99.3243	12.723	5.6603	20.8784	55.125	5.9459	34.5507	1.7048
Q96F46	866	99.4226	36.383	22.73	2.5115	21.1345	0.3176	8.177	1.0736
Q96JC1	886	99.4357	3.565	2.164	66.0835	82.9628	41.4221	63.5468	1.1447
Q96P20	1036	99.5174	14.659	6.1123	19.6911	55.3933	4.778	33.8694	2.4871
Q96PD4	163	96.9325	8.703	4.1108	43.5583	74.6242	22.8528	54.3942	0.506
Q99836	296	98.3108	8.761	5.2907	24.1554	46.6723	7.6858	26.2584	0.6246
Q9BV40	100	95.0	3.375	2.3022	62.5	77.55	38.0	59.6125	0.4611
Q9BYF1	480	98.9583	5.231	1.4446	67.0312	94.7708	43.125	80.4167	0.7056
Q9H074	479	98.9562	36.353	28.2003	1.4614	8.63	0.0522	2.44	0.738
Q9NR97	1041	99.5197	21.572	11.2926	6.4121	23.5387	1.3929	8.2841	2.3966
Q9NRS4	437	98.8558	6.429	2.8379	51.2586	85.5807	28.8902	70.7466	0.7937
Q9NVJ2	186	97.3118	1.744	1.2656	91.129	96.8683	72.8495	89.3952	0.6283
Q9ULC8	765	99.3464	38.808	32.3238	3.4314	7.8088	0.3922	1.8399	1.0204
Q9Y2I7	2098	99.7617	33.211	23.7625	5.8508	16.2095	0.9175	5.4469	3.7743
Q9Y397	364	98.6264	9.301	2.9895	44.9176	82.3867	23.3516	66.1504	0.6409

Table 10: Prediction confidence results using the reduced database AlphaFold configuration with  $L = 20$ . This is part I of II.

Protein ID	$n$	RMSD	$\mu_{\text{all}}$	$\sigma_{\text{all}}$	$\mu_{\text{diff}}$	$\sigma_{\text{diff}}$	$\mu'_{\text{all}}$	$\sigma'_{\text{all}}$	$\mu'_{\text{diff}}$	$\sigma'_{\text{diff}}$
A0A663	38	3.129	75.048	11.991	71.45	1.508	74.755	11.327	74.862	4.587
MPROTEI	193	2.06	89.041	7.416	87.138	2.009	87.461	8.837	73.19	3.874
NSP2NNN	546	19.561	74.536	17.778	92.656	1.044	73.385	17.646	91.094	1.21
NSP4NNN	494	11.389	83.936	8.896	89.444	1.356	83.913	8.92	87.668	1.288
NSP6NNN	290	8.921	77.331	11.445	73.286	2.769	76.104	12.64	65.228	0.762
O00327	626	10.445	65.242	25.756	32.584	3.532	65.128	25.804	32.296	1.221
O14745	358	12.34	72.042	17.526	88.666	0.565	72.051	17.223	70.686	7.533
O14786	923	33.465	79.024	21.94	36.21	1.406	78.925	21.993	35.662	2.1
O15393	492	24.847	80.455	20.693	41.292	2.675	80.765	20.643	41.088	3.315
O15455	904	24.886	90.367	14.664	96.286	1.564	90.261	14.604	91.518	0.356
O43765	313	12.051	79.03	20.468	88.548	3.314	79.191	20.501	88.86	2.758
O94826	608	11.824	79.953	25.515	25.302	1.419	80.241	26.177	24.912	2.005
O95721	258	8.478	75.906	22.281	89.91	0.914	75.923	21.394	89.766	1.254
O95786	925	33.92	83.194	16.732	88.724	1.844	83.717	16.674	86.648	2.241
O95992	272	6.531	91.633	13.904	96.86	0.666	91.815	14.142	96.806	0.787
P00973	400	7.988	83.749	21.993	89.328	1.047	83.832	21.867	90.164	0.926
P01185	164	5.552	79.569	16.773	86.778	1.34	78.21	16.506	79.71	1.177
P01889	362	9.904	87.936	18.463	47.662	2.89	87.711	18.817	42.058	1.925
P02649	317	16.897	75.319	18.538	45.584	0.691	74.833	19.063	43.904	3.122
P04233	296	17.217	70.433	20.278	90.33	2.496	69.938	20.327	87.284	3.829
P04439	365	9.016	86.959	19.05	43.686	2.588	87.121	19.044	44.268	3.233
P05109	93	1.953	92.956	10.483	98.21	0.266	93.971	10.54	97.618	0.329
P05161	165	2.557	86.236	11.269	88.324	3.105	87.591	10.99	92.202	0.684
P05231	212	7.214	84.805	16.694	58.22	1.7	84.561	17.821	57.118	5.322
P07711	333	8.263	93.679	11.289	96.096	0.739	93.987	9.796	92.25	2.42
P08887	468	11.083	78.202	23.606	48.592	1.57	78.237	23.467	40.974	4.313
P09429	215	24.633	76.632	23.082	87.266	1.572	76.506	22.79	85.194	1.507
P09958	794	24.603	85.088	20.744	55.2	2.152	85.213	20.625	48.182	2.726
P0DTC2	1273	10.44	78.887	16.851	43.964	11.301	78.793	17.001	41.546	12.094
P0DTC3	275	16.932	49.31	20.799	68.958	1.12	49.737	18.922	66.964	2.356
P0DTC4	75	3.403	74.108	15.66	86.564	2.455	70.975	16.037	78.342	3.36
P0DTC5	222	9.978	84.285	13.438	77.74	1.38	84.175	13.413	83.272	0.819
P0DTC6	61	5.379	86.46	13.406	97.194	0.606	84.249	13.294	88.176	2.458
P0DTC7	121	8.067	76.98	15.559	68.908	1.929	77.021	13.534	78.996	2.271
P0DTC8	121	17.706	80.17	13.321	50.0	2.248	60.707	22.596	35.768	1.302
P0DTC9	419	27.007	68.399	23.597	36.932	3.69	68.28	23.457	36.95	3.116
P0DTD2	97	4.388	79.607	16.769	92.54	0.706	79.076	16.655	91.874	0.678
P0DTD3	73	24.441	68.544	14.985	57.288	2.791	69.92	14.985	63.542	5.297
P0DTD8	43	2.458	89.464	10.491	85.754	6.336	89.428	10.44	84.788	2.948
P0DTF1	22	2.589	95.196	6.768	98.532	0.162	88.977	9.041	86.57	0.939
P0DTG0	57	12.352	47.494	6.446	46.364	2.274	51.696	8.039	54.49	2.471
P0DTG1	41	15.533	74.977	7.67	79.804	2.456	73.7	9.233	78.844	1.75
P11226	248	16.516	80.221	20.491	45.93	3.496	80.601	19.994	53.552	2.939
P13164	125	30.581	65.86	17.167	57.746	1.217	66.137	17.299	68.906	1.428
P13747	358	14.9	87.122	17.953	65.358	3.687	86.866	18.362	45.174	1.508
P17181	557	12.674	78.051	21.024	41.674	5.38	78.097	20.97	43.752	3.981
P17405	631	12.182	87.596	22.476	48.034	3.069	87.558	22.861	33.232	6.77
P20701	1170	10.129	82.3	16.239	31.852	2.669	82.095	16.892	24.556	1.216
P26022	381	15.865	79.175	19.768	54.22	5.098	77.667	21.36	42.768	2.566
P26715	233	30.415	74.997	23.568	36.586	0.839	73.933	24.603	38.216	4.465
P29597	1187	5.571	81.737	20.108	93.04	4.918	81.602	20.193	84.85	6.157
P30556	359	12.313	81.815	19.517	95.35	0.857	81.98	20.04	96.014	0.413
P33076	1130	30.469	68.876	27.612	25.838	1.988	69.022	27.382	27.406	2.7
P35232	272	2.652	88.354	9.295	88.634	0.647	87.474	10.562	65.122	2.361
P35613	385	9.773	86.321	16.975	41.688	2.507	86.056	17.439	41.862	2.688
P40189	918	22.039	75.005	25.376	73.17	2.298	74.838	25.38	67.82	2.657
P47901	424	17.192	73.874	23.532	86.392	2.649	73.475	24.844	84.59	2.816
P48551	515	36.573	62.979	23.882	52.708	2.159	63.525	23.313	54.156	2.675
P49327	2511	33.768	85.931	12.562	95.704	3.157	85.719	12.081	88.756	4.571
P49754	854	6.766	87.457	12.041	36.328	3.905	87.275	12.067	33.306	4.098
P51149	207	7.341	88.012	16.049	95.476	2.282	86.78	17.15	91.898	4.241

Table 11: Prediction confidence results using the reduced database AlphaFold configuration with  $L = 20$ . This is part II of II.

Protein ID	$n$	RMSD	$\mu_{\text{all}}$	$\sigma_{\text{all}}$	$\mu_{\text{diff}}$	$\sigma_{\text{diff}}$	$\mu'_{\text{all}}$	$\sigma'_{\text{all}}$	$\mu'_{\text{diff}}$	$\sigma'_{\text{diff}}$
P52292	529	9.065	87.35	19.082	64.18	15.207	87.229	19.347	49.878	11.916
P52948	1817	56.34	55.901	24.723	34.444	2.948	55.807	24.315	35.338	1.097
P56962	302	25.013	69.898	22.843	92.422	1.212	69.777	22.207	77.418	5.058
P59594	1255	4.432	80.532	15.908	91.996	0.605	80.352	16.139	90.166	0.838
P59595	422	26.286	68.249	23.318	34.632	2.009	67.744	23.489	32.506	1.776
P59596	221	9.173	82.821	13.832	78.104	1.736	81.492	14.351	73.706	2.18
P59632	274	18.052	48.927	18.922	42.85	3.674	47.395	18.279	42.27	4.011
P59633	154	20.183	44.815	10.281	29.56	1.883	44.543	8.393	53.31	1.047
P59634	63	2.5	81.663	14.713	93.518	1.588	81.059	14.849	94.688	0.757
P59635	122	5.955	76.497	14.537	68.356	1.203	75.91	15.363	65.254	1.946
P59636	98	3.095	81.38	15.126	71.648	10.347	81.841	14.977	76.852	7.67
P59637	76	1.743	74.234	15.368	64.032	4.852	74.108	15.208	64.31	4.526
P62937	165	1.011	98.113	2.587	98.798	0.041	96.965	3.335	87.938	2.755
P68104	462	1.511	88.394	9.591	91.838	1.624	89.146	8.709	93.526	1.249
P84022	425	20.077	83.642	20.642	43.472	6.192	83.347	20.759	50.382	7.638
PLRPOCT	355	3.898	89.417	6.968	95.582	1.071	89.169	7.102	93.628	1.188
Q01628	133	21.561	59.739	17.909	39.38	3.242	59.924	17.169	42.198	4.821
Q01629	132	12.883	64.634	18.829	46.14	2.997	63.584	17.401	63.314	3.207
Q10589	180	2.608	85.59	18.527	93.958	0.678	85.502	18.375	93.744	0.999
Q13241	179	7.989	87.206	17.061	60.99	1.353	87.482	16.715	67.312	3.281
Q13568	498	21.258	72.92	23.907	74.752	13.376	72.434	24.044	66.518	17.607
Q14653	427	20.062	79.763	20.779	93.28	0.882	79.651	21.805	93.232	2.073
Q16236	605	30.752	60.999	23.846	62.764	1.233	61.093	24.204	59.954	3.664
Q16552	155	17.781	85.666	13.867	88.084	2.369	84.281	15.2	59.232	2.148
Q16553	131	13.654	78.067	14.012	78.422	1.225	77.79	14.611	65.996	3.023
Q16665	826	44.207	59.826	27.36	73.512	6.532	60.058	27.234	78.47	5.483
Q4KMQ2	910	2.872	82.045	15.602	28.8	1.47	82.003	15.929	25.714	0.305
Q5BJD5	291	14.524	82.227	17.05	43.656	0.812	82.271	19.295	28.726	1.839
Q5W0Z9	365	21.394	85.075	23.832	97.328	0.902	85.184	23.538	95.796	1.3
Q7TFA0	39	14.095	78.255	18.387	88.616	7.838	77.564	15.863	78.662	8.313
Q7TFA1	44	2.214	86.231	14.568	86.222	5.632	85.982	14.676	83.248	6.791
Q7TLC7	70	24.421	68.985	15.09	81.236	2.675	68.248	14.198	62.218	4.773
Q7Z434	540	49.531	55.241	20.475	95.628	0.533	55.234	20.5	93.11	0.748
Q80H93	84	16.513	38.072	4.559	31.814	3.442	39.286	8.313	25.232	1.471
Q86U44	580	21.605	74.845	24.463	74.804	2.774	75.184	24.403	70.658	2.049
Q86WV6	379	18.481	83.715	17.147	97.19	0.445	83.659	16.647	89.116	2.238
Q8IUC6	712	28.425	63.163	24.255	92.834	0.495	62.983	24.05	89.902	0.656
Q8N3R9	675	31.253	76.968	23.045	34.854	3.227	77.127	22.825	23.624	3.007
Q8N884	522	22.258	77.629	25.586	37.216	2.518	77.417	25.721	36.742	1.888
Q8NAC3	791	11.777	73.601	21.263	46.174	1.626	73.381	21.494	35.99	1.497
Q8NEB9	887	21.53	84.277	16.464	94.73	0.876	83.94	16.618	91.312	2.225
Q8NHX9	752	7.509	79.975	17.879	33.494	2.312	80.029	17.636	42.968	5.183
Q92499	740	9.308	85.712	14.882	88.672	3.271	86.372	14.47	90.208	2.94
Q92985	503	26.943	68.348	24.663	88.68	1.901	68.228	24.289	61.53	6.459
Q96C10	678	2.133	90.875	8.282	97.724	0.86	90.487	8.719	91.106	5.603
Q96F46	866	42.175	69.056	26.075	54.104	3.17	68.987	26.091	34.054	1.728
Q96JC1	886	2.853	88.144	8.568	94.134	0.275	87.456	8.614	88.358	0.515
Q96P20	1036	12.888	80.863	19.484	89.236	1.108	80.791	19.538	84.994	1.66
Q96PD4	163	14.017	87.556	15.56	80.29	2.432	85.833	18.033	49.242	4.759
Q99623	299	8.752	84.62	11.565	84.124	2.261	85.089	12.409	83.036	4.335
Q99836	296	6.525	81.472	14.828	69.176	10.703	81.182	14.261	68.55	9.133
Q9BV40	100	3.427	89.359	13.065	93.94	0.823	88.458	12.435	92.318	0.979
Q9BYF1	480	5.509	92.351	10.146	51.158	1.636	92.898	9.614	52.218	3.92
Q9BYX4	1025	4.818	79.75	21.358	81.918	2.421	79.805	21.328	72.982	3.576
Q9C000	1473	35.861	69.449	25.846	86.358	4.214	69.717	25.962	72.072	4.221
Q9H074	479	30.3	72.33	24.787	57.078	4.864	71.602	26.038	42.676	2.225
Q9NR97	1041	21.869	87.848	14.307	54.966	4.4	87.815	14.379	56.082	2.013
Q9NRS4	437	6.233	87.694	13.102	90.044	2.06	87.436	13.579	89.578	1.338
Q9NVJ2	186	1.945	91.479	11.254	80.562	3.887	91.257	11.377	67.22	5.577
Q9NYK1	1049	12.803	87.369	15.844	59.046	4.871	87.454	15.725	48.7	3.93
Q9UHD2	729	5.063	89.556	13.939	97.104	1.418	89.359	14.059	95.536	1.129
Q9ULC8	765	34.128	57.602	26.325	97.412	0.375	57.685	26.027	96.774	0.453
Q9Y217	2098	34.987	64.043	28.71	28.668	1.65	64.029	29.133	21.178	0.918
Q9Y397	364	11.551	84.236	21.308	55.18	1.752	84.093	21.323	50.83	4.146

Table 12: Prediction confidence results using the full database AlphaFold configuration. This is part I of II.

Seq. ID	$n$	RMSD	$\mu_{\text{all}}$	$\sigma_{\text{all}}$	$\mu_{\text{diff}}$	$\sigma_{\text{diff}}$	$\mu'_{\text{all}}$	$\sigma'_{\text{all}}$	$\mu'_{\text{diff}}$	$\sigma'_{\text{diff}}$
A0A663	38	2.886	75.736	10.537	88.266	1.015	70.263	11.001	75.346	1.262
MPROTEI	193	5.562	87.9	7.153	92.318	1.308	87.857	6.955	88.774	1.525
NSP2NNN	546	22.333	83.737	12.059	94.264	1.16	83.833	11.752	91.19	0.457
NSP4NNN	494	16.995	81.696	9.823	89.742	1.546	81.481	9.997	88.32	1.986
NSP6NNN	290	5.41	78.09	12.781	79.708	2.607	77.337	11.29	81.604	1.085
O00327	626	18.69	65.332	25.637	34.454	4.124	65.298	26.183	29.684	3.145
O14745	358	7.395	71.834	17.666	87.546	0.83	71.453	17.52	71.164	6.795
O14786	923	36.546	79.032	21.688	36.114	1.665	79.167	21.792	37.798	2.439
O15393	492	19.978	80.703	21.253	35.588	3.047	80.475	21.314	38.482	2.24
O15455	904	20.539	89.822	14.659	93.75	0.576	89.897	14.681	88.368	1.734
O43765	313	14.438	80.221	19.634	94.786	1.027	80.554	19.423	93.71	1.392
O94826	608	8.407	81.232	25.994	24.44	1.076	81.309	25.374	24.338	1.394
O95721	258	11.099	76.044	20.028	94.472	1.042	75.623	20.744	89.75	0.788
O95992	272	5.988	91.775	13.799	96.072	0.75	91.048	13.976	90.196	1.92
P00973	400	14.825	83.661	22.121	87.986	2.211	83.888	22.197	88.732	1.671
P01185	164	7.641	79.565	16.968	54.8	2.856	79.506	16.961	55.752	3.383
P01889	362	9.441	87.63	18.772	44.886	1.572	87.651	18.719	46.628	2.721
P02649	317	22.675	74.197	18.551	44.938	1.656	74.255	17.582	44.798	2.96
P04233	296	18.279	68.498	20.332	90.584	2.164	68.742	20.641	89.472	1.721
P04439	365	6.162	86.845	18.995	44.23	2.704	86.921	19.068	44.678	3.968
P05109	93	1.19	94.633	10.47	96.582	2.721	94.62	10.248	90.894	6.768
P05161	165	2.569	85.182	10.732	87.384	3.029	85.738	10.568	90.89	0.545
P05231	212	9.402	85.294	16.248	57.324	4.406	84.919	17.756	55.27	3.901
P07711	333	7.479	93.624	11.188	96.6	0.67	93.941	9.784	92.306	2.45
P08887	468	10.171	79.042	23.058	50.664	1.41	79.053	23.11	44.186	3.148
P09429	215	20.391	75.711	23.003	94.868	0.426	76.624	22.933	93.982	0.536
P09958	794	32.057	85.332	20.268	55.18	2.153	85.024	20.889	36.474	0.395
P0DTC2	1273	4.917	78.96	16.515	44.794	11.075	78.972	16.515	41.002	13.017
P0DTC3	275	11.391	61.089	21.166	50.25	1.085	61.363	20.931	46.506	3.1
P0DTC4	75	2.496	75.297	15.67	91.574	1.843	74.004	15.183	82.986	3.486
P0DTC5	222	6.436	83.012	14.062	89.206	2.336	83.312	13.759	89.546	1.351
P0DTC6	61	4.88	86.241	12.854	96.814	0.676	84.169	13.171	89.606	2.674
P0DTC7	121	4.492	76.821	15.179	66.336	1.601	77.019	15.334	68.648	1.564
P0DTC8	121	17.601	56.598	10.34	63.222	3.508	48.462	12.791	53.566	2.139
P0DTC9	419	29.977	67.367	23.173	88.718	2.222	67.564	23.335	85.494	3.082
P0DTD2	97	4.156	79.424	16.645	92.134	0.784	78.68	16.368	90.232	0.666
P0DTD3	73	17.276	69.06	15.256	47.152	3.291	69.138	15.24	44.438	3.966
P0DTD8	43	2.394	89.893	10.325	85.21	6.189	89.745	10.28	83.602	3.102
P0DTF1	22	2.033	95.286	6.738	98.574	0.134	93.265	8.046	96.042	0.735
P0DTG0	57	13.398	46.508	6.478	44.294	2.44	47.424	5.993	47.484	1.588
P0DTG1	41	17.037	79.198	8.769	85.9	2.624	77.292	10.147	78.726	2.596
P11226	248	21.819	80.394	20.402	47.02	1.473	80.227	20.867	48.33	2.905
P13164	125	8.675	65.077	17.669	56.108	2.975	63.893	16.589	54.514	2.112
P13747	358	12.178	86.76	18.681	49.512	2.503	86.547	18.838	57.836	2.876
P17181	557	21.61	79.093	20.317	43.486	1.523	78.859	20.886	48.594	2.501
P17405	631	12.066	87.796	22.376	47.99	2.672	87.682	22.809	29.628	3.587
P20701	1170	8.323	82.167	16.158	32.766	0.935	82.255	16.678	24.696	1.215
P26022	381	14.411	80.061	19.401	50.256	4.399	79.295	19.914	37.094	2.276
P26715	233	22.384	74.56	23.912	36.474	1.217	74.551	24.108	34.286	1.773
P29597	1187	32.804	82.201	20.483	95.13	2.856	82.191	20.266	84.898	8.554
P30556	359	10.111	80.902	19.02	39.53	2.981	81.31	18.965	38.666	3.949
P33076	1130	26.719	69.118	27.69	52.374	5.287	69.073	27.682	69.802	1.087
P35232	272	3.447	88.919	9.067	88.67	1.189	88.485	8.855	87.73	1.575
P35613	385	8.896	85.87	17.193	43.738	2.005	86.146	17.188	46.344	2.166
P40189	918	24.632	74.808	25.439	75.236	2.187	74.814	25.51	68.942	3.959
P47901	424	5.702	74.001	23.301	88.66	2.375	74.045	23.157	85.132	2.005
P48551	515	28.717	64.011	23.755	70.534	3.521	63.891	23.481	61.75	2.599
P51149	207	6.188	88.239	16.587	95.512	2.591	87.067	17.216	91.842	4.365

Table 13: Prediction confidence results using the full database AlphaFold configuration. This is part II of II.

Seq. ID	$n$	RMSD	$\mu_{\text{all}}$	$\sigma_{\text{all}}$	$\mu_{\text{diff}}$	$\sigma_{\text{diff}}$	$\mu'_{\text{all}}$	$\sigma'_{\text{all}}$	$\mu'_{\text{diff}}$	$\sigma'_{\text{diff}}$
P56962	302	22.301	69.172	23.753	96.516	0.409	69.342	23.759	96.54	0.463
P59596	221	7.506	82.061	12.733	76.868	1.775	81.175	13.742	72.064	2.043
P59632	274	13.018	58.367	18.783	66.136	2.029	57.364	18.794	60.926	4.362
P59633	154	20.993	47.859	10.608	38.736	4.455	46.228	8.664	48.764	0.907
P59634	63	2.514	81.124	14.464	91.134	2.227	79.701	14.365	84.632	4.937
P59635	122	6.527	76.232	15.74	69.514	0.897	76.129	16.043	54.806	3.045
P59636	98	5.647	80.765	16.225	91.182	5.274	77.654	15.556	79.584	6.025
P59637	76	3.488	75.038	15.62	66.71	6.263	75.677	15.389	65.872	5.204
P62937	165	0.963	98.037	2.658	98.78	0.11	97.592	2.813	96.842	1.058
P68104	462	1.547	87.439	10.419	90.584	1.789	88.26	9.399	93.154	1.275
P84022	425	16.633	83.759	20.532	45.254	6.648	83.581	20.67	41.162	5.792
PLRPOCT	355	3.824	90.168	6.528	92.868	1.836	89.47	7.723	84.62	3.832
Q01628	133	26.947	59.485	12.738	55.092	3.368	60.204	15.275	49.082	4.223
Q01629	132	18.508	62.633	17.46	77.596	2.819	62.329	17.48	70.92	1.877
Q10589	180	11.884	84.566	17.867	93.704	0.746	83.726	18.104	90.02	1.893
Q13241	179	11.456	87.467	17.008	93.192	0.895	87.165	16.87	88.192	1.946
Q13568	498	29.991	72.656	23.921	92.118	0.769	72.434	23.764	79.794	5.125
Q14653	427	16.703	79.881	21.726	88.028	4.931	79.761	22.05	89.036	3.51
Q16236	605	38.828	60.894	24.052	70.194	0.603	60.396	24.197	51.342	4.096
Q16552	155	13.575	83.831	14.869	87.152	2.516	83.098	15.725	56.958	4.194
Q16553	131	10.901	78.582	14.393	78.83	0.746	78.854	14.611	69.338	1.745
Q16665	826	41.354	59.753	27.088	84.802	2.557	59.815	26.839	83.638	2.931
Q4KMQ2	910	4.59	81.331	15.895	29.766	1.54	81.46	15.823	28.168	3.134
Q5BJD5	291	13.792	82.742	17.059	43.9	1.158	82.653	19.347	27.804	1.888
Q5WOZ9	365	15.887	85.224	23.712	98.5	0.087	85.247	23.511	97.632	0.322
Q7TFA0	39	2.505	78.834	15.988	87.908	9.073	79.225	15.951	89.984	5.317
Q7TFA1	44	2.106	85.691	14.274	84.248	5.805	85.609	14.322	82.498	5.857
Q7TLC7	70	24.995	70.072	14.57	52.722	2.59	70.101	14.933	45.152	2.867
Q7Z434	540	50.815	55.255	20.386	95.978	0.55	55.05	19.831	85.694	3.344
Q80H93	84	14.707	63.83	6.81	71.14	1.769	52.502	12.869	40.918	1.147
Q86U44	580	17.742	74.735	24.442	35.918	1.898	74.552	24.301	31.652	0.349
Q86WV6	379	20.858	83.949	16.754	96.908	0.31	83.971	16.467	89.178	2.384
Q8IUC6	712	49.827	62.905	24.297	93.142	0.412	62.708	23.747	84.022	1.321
Q8N3R9	675	35.139	78.299	22.289	55.756	7.659	78.394	22.344	56.592	5.767
Q8N884	522	29.73	77.606	25.97	38.534	3.736	77.404	26.054	36.74	1.55
Q8NAC3	791	11.202	74.645	21.198	41.694	2.118	74.661	21.317	35.41	3.997
Q8NHX9	752	6.888	80.556	17.278	91.308	0.553	80.289	17.483	87.504	0.721
Q92499	740	12.723	86.385	14.576	89.098	1.926	86.362	14.876	88.688	1.804
Q96F46	866	36.383	68.955	26.798	49.514	2.823	68.911	26.894	36.258	3.614
Q96JC1	886	3.565	88.113	8.225	93.376	0.356	88.239	8.657	91.282	0.696
Q96P20	1036	14.659	80.375	19.634	23.954	2.496	80.21	19.724	24.76	1.336
Q96PD4	163	8.703	87.758	14.681	82.896	1.929	86.532	16.772	56.214	6.728
Q99836	296	8.761	81.213	13.817	78.914	7.454	80.918	13.971	72.198	6.253
Q9BV40	100	3.375	89.26	11.772	96.458	0.289	84.495	13.064	85.25	2.311
Q9BYF1	480	5.231	92.48	10.124	48.952	1.565	92.981	9.549	53.718	4.395
Q9H074	479	36.353	72.107	25.823	56.444	4.022	71.939	25.903	41.594	2.434
Q9NR97	1041	21.572	87.692	14.66	60.438	3.784	86.732	15.638	35.11	2.076
Q9NRS4	437	6.429	87.475	13.523	57.542	2.717	87.623	13.176	59.396	2.244
Q9NVJ2	186	1.744	92.241	10.762	78.798	6.333	91.723	11.576	55.84	2.358
Q9ULC8	765	38.808	57.841	25.532	97.696	0.34	57.592	25.77	97.14	0.448
Q9Y2I7	2098	33.211	64.167	27.302	27.08	0.878	64.111	27.934	23.858	0.46
Q9Y397	364	9.301	83.666	21.359	55.914	2.097	83.822	21.283	52.324	3.18



Table 14: GDT-TS results based on AlphaFold predefined confidence regions using the full database AlphaFold configuration. Regions  $R_1$  to  $R_4$  correspond to confidence scores of above 90%, 70% to 90%, 50% to 70%, and below 50%, respectively. This is part I of II.

Seq. ID	$n$	$R_1$ GDT (%)	$R_1$ (%)	$R_2$ GDT (%)	$R_2$ (%)	$R_3$ GDT (%)	$R_3$ (%)	$R_4$ GDT (%)	$R_4$ (%)
A0A663	38	N/A	0.0	89.815	71.053	65.909	28.947	N/A	0.0
MPROTEI	193	38.918	50.259	36.648	45.596	31.25	4.145	N/A	0.0
NSP2NNN	546	8.447	40.11	9.449	46.52	3.448	10.623	8.333	2.747
NSP4NNN	494	5.67	19.636	9.91	67.409	2.917	12.146	6.25	0.81
NSP6NNN	290	85.227	7.586	76.279	74.138	42.143	12.069	11.111	6.207
O00327	626	21.014	33.067	8.43	13.738	7.188	12.78	2.767	40.415
O14745	358	32.927	11.453	26.117	50.0	22.619	23.464	8.333	15.084
O14786	923	1.244	43.554	0.949	34.236	0.0	4.659	1.235	17.551
O15393	492	11.643	56.301	7.692	21.138	16.176	6.911	0.974	15.65
O15455	904	10.731	72.677	0.872	19.027	2.083	3.982	8.333	4.314
O43765	313	17.296	50.799	11.194	21.406	12.5	14.696	7.317	13.099
O94826	608	57.007	69.243	67.727	9.046	40.385	2.138	11.555	19.572
O95721	258	44.196	43.411	34.694	18.992	22.273	21.318	10.714	16.279
O95992	272	58.798	85.662	41.25	7.353	25.0	1.471	10.0	5.515
P00973	400	27.099	65.5	28.929	17.5	23.438	4.0	2.404	13.0
P01185	164	35.959	44.512	27.703	22.561	32.292	29.268	20.833	3.659
P01889	362	69.069	75.691	24.074	7.459	14.286	5.801	25.0	11.05
P02649	317	3.883	32.492	2.151	29.338	1.761	22.397	0.5	15.773
P04233	296	25.725	23.311	26.765	28.716	27.869	20.608	8.642	27.365
P04439	365	58.086	73.699	36.719	8.767	16.304	6.301	18.902	11.233
P05109	93	97.126	93.548	100.0	1.075	91.667	3.226	62.5	2.151
P05161	165	90.678	35.758	79.62	55.758	41.667	5.455	50.0	3.03
P05231	212	37.316	64.151	25.781	15.094	5.263	17.925	4.167	2.83
P07711	333	47.518	84.685	38.71	9.309	5.769	3.904	0.0	2.102
P08887	468	47.94	57.051	41.667	12.179	17.188	6.838	11.607	23.932
P09429	215	12.371	45.116	7.273	25.581	1.667	6.977	0.521	22.326
P09958	794	6.733	66.877	2.009	14.106	0.0	6.549	0.505	12.469
PODTC2	1273	93.421	28.358	86.278	49.804	69.966	11.705	34.109	10.134
PODTC3	275	50.0	1.091	40.551	46.182	25.568	16.0	15.099	36.727
PODTC4	75	63.095	28.0	85.87	30.667	73.333	40.0	25.0	1.333
PODTC5	222	72.917	37.838	69.393	48.198	53.125	7.207	43.333	6.757
PODTC6	61	55.0	57.377	60.0	24.59	59.091	18.033	N/A	0.0
PODTC7	121	78.571	17.355	63.492	52.066	47.917	19.835	44.231	10.744
PODTC8	121	N/A	0.0	37.5	1.653	13.202	73.554	10.833	24.793
PODTC9	419	4.762	15.036	7.902	41.527	4.082	11.695	1.88	31.742
PODTD2	97	76.163	44.33	69.643	28.866	56.667	15.464	29.545	11.34
PODTD3	73	0.0	12.329	4.63	36.986	2.679	38.356	13.889	12.329
PODTD8	43	93.333	69.767	85.0	23.256	75.0	6.977	N/A	0.0
PODTF1	22	96.053	86.364	66.667	13.636	N/A	0.0	N/A	0.0
PODTG0	57	N/A	0.0	N/A	0.0	28.333	26.316	15.476	73.684
PODTG1	41	N/A	0.0	8.088	82.927	3.571	17.073	N/A	0.0
P11226	248	15.741	54.435	1.515	13.306	0.0	15.726	0.61	16.532
P13164	125	36.765	13.6	43.966	23.2	33.5	40.0	6.897	23.2
P13747	358	34.457	74.581	17.857	5.866	8.594	8.939	3.289	10.615
P17181	557	25.722	49.731	11.822	23.16	8.696	8.259	0.476	18.851
P17405	631	72.793	82.567	50.0	0.634	33.333	2.377	9.066	14.422
P20701	1170	50.441	38.803	52.667	44.872	41.912	8.718	9.831	7.607
P26022	381	34.637	46.982	10.476	27.559	0.521	12.598	3.571	12.861
P26715	233	22.458	50.644	3.261	9.871	2.0	10.73	1.119	28.755
P29597	1187	4.882	53.496	2.594	29.233	1.364	4.634	4.0	12.637
P30556	359	30.307	49.861	23.969	27.019	15.278	10.028	4.255	13.092
P33076	1130	23.591	36.106	13.542	25.487	9.551	7.876	3.043	30.531
P35232	272	69.591	62.868	58.523	32.353	8.333	3.309	18.75	1.471
P35613	385	32.722	67.273	28.175	16.364	7.292	6.234	1.282	10.13
P40189	918	44.341	49.564	22.619	18.301	12.162	4.031	4.651	28.105
P47901	424	61.08	41.509	61.48	23.113	56.618	8.019	21.121	27.358
P48551	515	17.383	24.854	17.391	17.864	6.553	20.0	1.302	37.282
P51149	207	42.007	71.014	38.889	13.043	27.381	10.145	2.083	5.797

Table 15: GDT-TS results based on AlphaFold predefined confidence regions using the full database AlphaFold configuration. Regions  $R_1$  to  $R_4$  correspond to confidence scores of above 90%, 70% to 90%, 50% to 70%, and below 50%, respectively. This is part II of II.

Seq. ID	$n$	$R_1$ GDT (%)	$R_1$ (%)	$R_2$ GDT (%)	$R_2$ (%)	$R_3$ GDT (%)	$R_3$ (%)	$R_4$ GDT (%)	$R_4$ (%)
P56962	302	28.958	39.735	5.952	6.954	4.583	19.868	2.97	33.444
P59596	221	37.5	26.244	36.94	60.633	20.0	6.787	5.357	6.335
P59632	274	N/A	0.0	34.184	35.766	35.87	25.182	14.72	39.051
P59633	154	N/A	0.0	N/A	0.0	11.486	48.052	4.688	51.948
P59634	63	91.071	44.444	76.471	26.984	84.722	28.571	N/A	0.0
P59635	122	54.762	17.213	39.286	51.639	29.167	19.672	19.643	11.475
P59636	98	61.735	50.0	46.875	24.49	22.368	19.388	16.667	6.122
P59637	76	88.889	23.684	61.607	36.842	53.571	36.842	25.0	2.632
P62937	165	100.0	98.788	100.0	0.606	100.0	0.606	N/A	0.0
P68104	462	98.235	55.195	90.123	35.065	80.682	9.524	50.0	0.216
P84022	425	40.67	64.941	27.692	15.294	6.25	4.706	2.734	15.059
PLRPOCT	355	79.418	65.352	67.308	32.958	100.0	1.69	N/A	0.0
Q01628	133	N/A	0.0	12.069	21.805	3.788	49.624	1.974	28.571
Q01629	132	N/A	0.0	28.509	43.182	10.938	24.242	3.488	32.576
Q10589	180	16.176	66.111	5.556	10.0	1.471	18.889	5.556	5.0
Q13241	179	24.031	72.067	30.0	11.173	22.222	10.056	12.5	6.704
Q13568	498	2.128	37.751	0.909	22.088	1.471	10.241	0.168	29.92
Q14653	427	34.502	51.756	30.787	25.293	29.167	5.621	8.784	17.33
Q16236	605	5.37	22.314	6.796	17.025	7.857	11.57	2.609	49.091
Q16552	155	35.473	47.742	6.122	31.613	3.226	20.0	0.0	0.645
Q16553	131	71.809	35.878	30.814	32.824	35.256	29.771	25.0	1.527
Q16665	826	16.599	29.903	15.845	8.596	6.25	10.654	1.131	50.847
Q4KMQ2	910	94.659	37.033	85.238	46.154	70.789	10.44	19.397	6.374
Q5BJD5	291	33.562	50.172	24.107	28.866	31.452	10.653	5.0	10.309
Q5WOZ9	365	28.71	77.534	0.0	3.014	5.0	1.37	0.0	18.082
Q7TFA0	39	98.529	43.59	86.111	23.077	72.917	30.769	100.0	2.564
Q7TFA1	44	100.0	59.091	97.5	22.727	87.5	18.182	N/A	0.0
Q7TLC7	70	6.818	15.714	2.941	24.286	0.61	58.571	0.0	1.429
Q7Z434	540	20.699	17.222	2.941	3.148	1.768	18.333	0.755	61.296
Q80H93	84	N/A	0.0	23.864	26.19	15.984	72.619	0.0	1.19
Q86U44	580	24.507	35.0	25.377	34.31	20.0	6.897	15.036	23.793
Q86WV6	379	15.183	57.784	9.184	25.858	8.929	7.388	1.471	8.971
Q8IUC6	712	1.25	22.472	1.415	22.331	1.953	8.989	2.052	46.208
Q8N3R9	675	4.646	50.222	4.012	24.0	4.327	7.704	4.713	18.074
Q8N884	522	33.075	61.686	21.711	7.28	2.778	1.724	2.288	29.31
Q8NAC3	791	45.924	23.262	39.034	48.42	37.338	9.735	14.286	18.584
Q8NHX9	752	70.312	36.17	64.201	44.947	55.634	9.441	30.282	9.441
Q92499	740	21.651	56.486	20.366	31.351	28.061	6.622	7.317	5.541
Q96F46	866	5.689	38.568	1.355	19.169	0.455	6.351	0.08	35.912
Q96JC1	886	82.195	53.725	70.013	42.438	33.654	2.935	0.0	0.903
Q96P20	1036	21.785	43.533	18.311	35.714	16.463	7.915	18.421	12.838
Q96PD4	163	57.87	66.258	18.333	18.405	13.636	13.497	0.0	1.84
Q99836	296	36.574	18.243	24.611	65.203	9.375	10.811	7.353	5.743
Q9BV40	100	65.441	68.0	62.5	22.0	43.75	8.0	37.5	2.0
Q9BYF1	480	67.651	79.375	78.165	16.458	20.455	2.292	0.0	1.875
Q9H074	479	1.442	43.424	1.087	14.405	1.63	9.603	1.763	32.568
Q9NR97	1041	13.689	62.632	5.163	26.513	2.5	5.764	0.472	5.091
Q9NRS4	437	61.032	64.302	47.087	23.57	28.906	7.323	0.0	4.805
Q9NVJ2	186	97.203	76.882	68.75	17.204	80.556	4.839	75.0	1.075
Q9ULC8	765	17.801	24.967	11.885	7.974	6.557	7.974	0.996	59.085
Q9Y2I7	2098	8.654	26.025	10.209	27.312	6.046	7.293	0.938	39.371
Q9Y397	364	56.687	66.758	36.17	12.912	20.0	6.868	7.653	13.462
Q9Y6K9	419	23.848	51.79	30.612	23.389	18.0	5.967	10.127	18.854